Construction and Building Materials 411 (2024) 134260

Contents lists available at ScienceDirect

Construction and Building Materials

journal homepage: www.elsevier.com/locate/conbuildmat

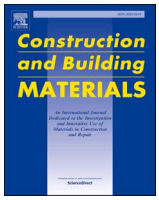

Experimental study and thermodynamic modelling of the temperature effect on the hydration of belite-ye'elimite-ferrite cements

Maruša Mrak [a,b], Frank Winnefeld [c], Barbara Lothenbach [c,d], Andraž Legat [a], Sabina Dolenec [a,*]

[a] Slovenian National Building and Civil Engineering Institute, Dimičeva ulica 12, 1000 Ljubljana, Slovenia
[b] Jožef Stefan International Postgraduate School, Jamova cesta 39, 1000 Ljubljana, Slovenia
[c] Empa, Swiss Laboratories for Materials Science and Technology, Überlandstrasse 129, 8600 Dübendorf, Switzerland
[d] Norwegian University of Science and Technology (NTNU), Department of Structural Engineering, Trondheim, Norway

ARTICLE INFO

Keywords:
Belite-ye'elimite-ferrite cement
Temperature
Hydration
Thermodynamic modelling

ABSTRACT

This study focuses on the kinetics of hydration, phase assemblage, microstructure and mechanical properties after various hydration times of two different BCSA cements at 5, 20, 40 and 60 °C and compares experimental data with thermodynamic modelling. Different curing temperatures change the type of hydrates and their amounts. Ye'elimite and gypsum in belite-ye'elimite-ferrite cements are almost fully reacted after 24 h of hydration at 20, 40 and 60 °C, while not at 5 °C. The hydration of belite is slower than the one of ye'elimite, but reaches a high degree of hydration after 150 days which is increasing with temperature. Less ettringite is present at elevated temperatures due to its increasing solubility, while more monosulfate is observed. Furthermore, with increasing temperature siliceous hydrogarnet forms at the expenses of strätlingite as well as more C–S–H is found as more belite reacts resulting in higher compressive strength. Dense and homogenous microstructure is observed at 5 °C, while it is more heterogeneous at higher temperatures. The presence of more ye'elimite resulted in higher ettringite and strätlingite formation and a higher compressive strength, while more belite yields more C–S–H in the hydrates and lower compressive strength.

1. Introduction

The hydration of cements is a temperature-sensitive process, which is not only influenced by different temperatures due to the external environment but also by heat produced by an exothermic reaction between cement and water [1–5]. The influence of temperature on the hydration of cements is a complex and important factor in understanding the behaviour and properties of cementitious materials [6].

Studies of the influence of temperature on the kinetics of Portland cement and blended Portland cement hydration have shown that the hydration kinetics of cement pastes is enhanced at elevated temperatures leading to increased early strength [1,5,7–10], while low temperatures reduce the hydration rate [11]. Elevated temperatures significantly modify the stability of hydrate phases [1,2]. At elevated temperatures, ettringite and monocarbonate are less stable due to the increased solubility of ettringite at high temperatures, compared to monosulfate and calcite [1,12,13]. It was also shown that at low temperatures ettringite forms a solid solution with carbonates [1]. Temperature also influences the crystallinity of aluminium hydroxide. At room temperature and below, nanocrystalline amorphous aluminium hydroxide is formed, while above 60 °C, the less soluble gibbsite is formed [13]. It has been reported that a denser and homogenous matrix is promoted at low temperatures, due to the slow but ongoing hydration. In addition, lower temperatures are associated with increased gel porosity in C-S-H and its lower density. [2,4,14,15].

Recent investigations on calcium sulfoaluminate cements showed that elevated temperatures enhance hydration [16–18], which was already confirmed for Portland cements. Different curing temperatures do not change the type of hydrates, however, they do impact the amounts of hydrates formed. [16]. Ettringite is reported to be stable in the absence of monocarbonate up to approximately 90 °C in ye'elimite-rich calcium sulfoaluminate cements, which can positively influence the compressive strength of cements pastes [19,20]. The compressive strength at early ages increases at elevated temperatures [16]. The porosity of calcium sulfoaluminate cement is gradually decreased at low temperatures, while the microstructure is less heterogenous [17,21], similar to Portland cements.

Compared to Portland cement and ye'elimite-rich calcium

* Corresponding author.
E-mail address: sabina.dolenec@zag.si (S. Dolenec).

https://doi.org/10.1016/j.conbuildmat.2023.134260
Received 17 July 2023; Received in revised form 11 November 2023; Accepted 18 November 2023
Available online 25 November 2023

sulfoaluminate cement, investigations on the effect of temperature on the hydration of belite-rich calcium sulfoaluminate cements are limited. A recent study by Chitvoranund [22] investigated the influence of temperature on the hydration and microstructure, using a two-phase belite-ye'elimite cement showing the accelerated hydration kinetics of ye'elimite at all temperatures resulting in the formation of ettringite, monosulfate and Al(OH). At later ages, due to higher reaction of belite at 5 and 60 °C C−S−H formed, while at 20 and 40 °C just strätlingite was present. Just a small amount of siliceous hydrogarnet was observed at 60 °C, due to the low amount of Fe present in the system. However, as regards belite-ye'elimite-ferrite cements, the influence of temperature was studied by Chen and Juenger [23], but the only method used besides compressive strength was isothermal calorimetry, without information on the hydration products formed. The outcome was similar to findings for ordinary Portland cement and blended Portland cements, namely increasing temperatures enhance the strength development, while at low temperatures the hydration is slower. Our previous research [24] has been focused on the hydration of belite-ye'elimite-ferrite cements, yet only at ambient and elevated temperatures, while lower temperatures (e.g. 5 °C) were not investigated. In addition, a low water to cement ratio and a very high calcium sulphate to ye'elimite molar ratio were implemented in that study leading to a lack of water for complete hydration [24]. Early hydration reactions at 25, 40 and 60 °C up to 1 day were studied with in situ X-ray diffraction analysis [25]. It was observed that early ye'elimite reaction was significantly accelerated at elevated temperatures. Temperature also decreased the crystallite size of ettringite, the main hydration product, due to its faster precipitation. Belite-ye'elimite-ferrite cement hydrated at 60 °C had larger ettringite crystals and a higher degree of reaction compared to samples cured at ambient temperature, resulting in higher compressive strength.

While there has been significant research on belite-ye'elimite-ferrite cement at ambient temperature, there are still some gaps in understanding the behaviour of belite-ye'elimite-ferrite cement at different temperatures, particularly in terms of low temperatures and the effects on mechanical properties and microstructure. This study examines the effects of low, ambient and increased curing temperatures on the phase development, microstructure and hydration kinetics of belite-ye'elimite-ferrite cements. Systematical microstructural and detailed EDS analyses at different temperatures were performed, which was not done previously, in order to improve the understanding of the development of hydration products at different temperatures. In addition, thermodynamic calculations of belite-ye'elimite-ferrite systems at different temperatures were not made available previously in the open literature. Thus valuable insights into the behaviour of belite-ye'elimite-ferrite cements in different curing environments will be provided which expand our understanding of the hydration mechanisms of belite-ye'elimite-ferrite cements.

The hydration of two belite-ye'elimite-ferrite cements was investigated at temperatures between 5 °C and 60 °C using experimental data and thermodynamic modelling. Hydration kinetics is studied by isothermal calorimetry, and compressive strength is determined on mortars. The hydrate assemblage of two cements with different phase compositions is investigated by X-ray powder diffraction, thermogravimetric analysis and energy-disperse X-ray microanalysis. The microstructure is assessed by scanning electron microscopy. Based on the experimental data a thermodynamic model is established to calculate the stable hydrate assemblage depending on temperature and dissolution kinetics.

2. Materials and methods

2.1. Materials

Two belite-ye'elimite-ferrite cement clinkers with different targeted phase compositions were synthesised. Clinker CBYF-B was targeted at 65 wt% belite (C_2S), 20 wt% ye'elimite ($C_4A_3\overline{S}$) and 10 wt% ferrite (C_4AF), and clinker CBYF-Y at 50 wt% belite (C_2S), 35 wt% ye'elimite ($C_4A_3\overline{S}$) and 10 wt% ferrite (C_4AF).

The clinkers were prepared of the following raw materials: limestone (Salonit Anhovo quarry), flysch (Salonit Anhovo quarry), bottom ash (Monfalcone power plant), white titanogypsum (Cinkarna Celje), calcined bauxite (Calucem) and mill scale (SIJ Acroni). The synthesis of the clinkers is described in detail in Borštnar et al. [24]. The chemical compositions of cement clinkers determined by X-ray fluorescence according to EN 196–2 and the mineralogical compositions derived from quantitative X-ray diffraction were already been reported in Mrak et al. [26]. The mineralogical and phase compositions are shown in Tables 1 and 2 below. CBYF-B contains more belite and less ye'elimite than CBYF-Y. The amorphous content in the cement clinker and anhydrous cement was not considered.

The Blaine specific surface areas of the cement clinkers were 4740 cm^2/g (specific density 3.18 g /cm^3) for cement clinker CBYF-B and 4250 cm^2/g (specific density 3.07 g /cm^3) for CBYF-Y [26].

The cement mixtures BYF-B and BYF-Y were prepared by blending the ground clinkers with 6.7 wt% and 12.5 wt% natural gypsum, respectively (composed of 96.7 wt% gypsum and 3.3 wt% anhydrite and ground below 0.063 mm), equating to an M-value (calcium sulphate to ye'elimite molar ratio) of 1.5 in each cement [26]. The particle size distributions of both the clinkers and the gypsum have previously been presented by Mrak et al. [26].

Prior to use, the raw materials were stored for 24 h at 5, 20, 40 and 60 °C. The cement pastes were prepared using a water-to-cement ratio of 0.5. They were mixed manually for 3 min using a spatula and the appropriate amount of water, filled into 15 ml polyethylene vials, then tightly sealed and cured at the respective temperatures.

The hydration of the cement pastes was stopped at specific time intervals 1, 7, 28 and 150 days by solvent exchange using isopropanol and diethyl ether. The crushed samples were for 15 min immersed in isopropanol, filtered with a Büchner funnel, then rinsed once with isopropanol and twice with diethyl ether and dried for 8 min at 40 °C to evaporate any remaining solvent, following the protocol described by Snellings et al. [27]. The dry pastes were investigated by scanning electron microscopy, while for X-ray powder diffraction and thermogravimetric analysis, pastes were ground to a particle size of below 0.063 mm by hand using an agate mortar and analysed afterward. It should be noted that results of the hydration experiments of cement mixtures BYF-B and BYF-Y at 20 ºC presented in the latter part of this work have been reported previously in [26].

Table 1
Chemical analyses of the BCSA clinkers and gypsum, wt% (WD-XRF, fused beads).

	CBCSA-B	CBCSA-Y	Gypsum
CaO	55.17	51.23	33.87
SiO_2	22.21	16.90	0.32
Al_2O_3	12.15	19.55	0.05
Fe_2O_3	3.62	3.66	0.04
MgO	1.53	1.28	0.39
K_2O	0.68	0.52	<0.04
Na_2O	0.29	0.23	<0.06
TiO_2	0.674	1.068	<0.016
P_2O_5	0.092	0.091	0.006
Cr_2O_3	0.083	0.078	0.002
MnO	0.060	0.047	0.003
SO_3	2.93	4.88	44.25
L.O.I. 1)	0.31	0.24	21.02
Total	99.77	99.76	99.95

1) Loss on ignition

Table 2
Phase compositions of cement clinkers determined by X-ray powder diffraction and Rietveld refinement in wt%. Data reproduced from [26].

	CBYF-B	CBYF-Y
β-Dicalcium silicate (belite)	60.6	50.9
γ-Dicalcium silicate	6.9	0.8
Ye'elimite orthorhombic	6.9	17.4
Ye'elimite cubic	9.3	14.9
∑ Ye'elimite	16.2	32.3
Ferrite	11.9	10.4
Mayenite	2.4	3.2
Periclase	1.0	1.0
Gehlenite	0.4	-
Perovskite	-	1.0
Aphthitalite	0.3	0.2
Arcanite	0.3	0.2

2.2. Methods

2.2.1. Isothermal calorimetry

Isothermal conduction calorimetry was performed at 5, 20, 40 and 60 °C using a Thermometric TAM Air (TA instruments). 4 g of the prepared cement and 2 g of deionized water, corresponding to a water-to-cement ratio of 0.5, were manually mixed for 3 min using a spatula, transferred into a glass ampoule, capped, and then placed directly into the calorimeter before being measured for 168 h. The early heat of hydration (up to approximately 30 min) could not be observed due to the external mixing procedure.

2.2.2. X-ray powder diffraction

X-ray powder diffraction was conducted using a PANalytical X'Pert Pro X-ray powder diffractometer equipped with $CuK_{\alpha 1}$ radiation (Johannson Ge (111) incident beam monochromator) and an X'Celerator detector at a voltage of 45 kV and a current of 40 mA. Samples were prepared by back-loading the powder into a circular sample holder with a diameter of 27 mm to minimise the preferred orientation effects. Samples were measured in a 2θ range of 5–75° with a step size of 0.017°2θ, using a 1° divergence slit and a 15 mm mask. The Rietveld refinement was performed using PANalytical X'Pert High Score Plus diffraction software (version 4.9). Crystal structures suggested by Snellings [28] were used, while the structures for orthorhombic and cubic ye'elimite were taken from Cuesta et al. [29,30]. The G-factor method [31–33] was used for the quantification of amorphous content and poorly crystalline phases with CaF_2 (Sigma Aldrich) used as the external standard. The results were normalised to 100 g of dry binder, including the amount of bound water determined from thermogravimetric analysis. The (free) water content in the XRD analysis was determined as follows: initially, an amount of 50 g of water was added to 100 g of dry binder (to achieve a water-to-cement ratio of 0.5), totalling 150 g. Subsequently, the content of all the phases derived from the XRD analysis was subtracted from this total. The resulting value represented the amount of water present.

2.2.3. Thermogravimetric analysis

Thermogravimetric (TGA) analysis was carried out using a Mettler Toledo TGA/SDTA 851^e. Measurements were carried out in the temperature range from 30° to 980°C with a heating rate of 20 K/min under a nitrogen atmosphere. Approximately 50 mg of the samples were placed in 150 µl alumina crucibles. Chemically bound water was calculated from the weight loss up to 550 °C and normalised to 100 g of dry binder [34].

2.2.4. Scanning electron microscopy and energy dispersive X-ray spectroscopy

Cross-sections of selected cement pastes (cured for either 150 days at 5, 20, 40 and 60 °C or 1, 7, 28 and 150 days at 20 °C), impregnated with epoxy resin, coarse polished using silicon carbide abrasive papers, fine polished using diamond paste and finally carbon coated, were examined by scanning electron microscopy (JEOL JSM-IT500) under high vacuum mode using backscattered electron mode (BSE). Imaging was performed with a backscattered electron detector at an accelerating voltage of 15 kV, and energy-dispersive X-ray microanalyses (EDS) were performed to identify the hydrates and their chemical composition. Over 100 points were analyzed per sample (matrix of hydrated cement pastes). Graphs of different atomic ratios of elements (Al/Ca, S/Ca, Si/Ca and Ca/Si) were utilised to illustrate trends in the composition of the hydration products.

2.2.5. Compressive strength

Mortars were prepared using quartz sand (CEN-Standard Sand EN 196–1 - Normensand with grain sizes between 0.1 and 2 mm), a cement/sand ratio of 25/75 by mass and a water-to-cement ratio of 0.5. They were mixed according to EN 196–1, cast in 25 mm × 25 mm x 25 mm moulds and then cured at 5, 20, 40 and 60 °C and a relative humidity of 95 ± 2%. The samples were demoulded after 24 h. After 1, 7, 28 and 150 days, the compressive strengths of the samples were determined using an LFM 50 (Walter + Bai) testing machine at a loading rate of 0.2 MPa/s, on three cubes per measurement age.

2.2.6. Thermodynamic modelling

Geochemical modelling was carried out to predict the type and amount of hydration products at various temperatures. The geochemical software GEMS [35,36] coupled with the cement-specific Cemdata18 database [13] was used. All thermodynamic calculations were done under oxidising conditions. For the C−S−H, the CSHQ model from Kulik [37] was used as detailed in [13], which accounts for the uptake of Na and K in C-S-H but neglects Al-binding by C-S-H.

First, the changes in phase volumes with ongoing hydration were calculated at respective temperatures (5, 20, 40 and 60 °C). The dissolution degrees of clinker phases at different hydration times, which were obtained by X-ray powder diffraction, were fitted using the following empirical non-linear equation (Eq. 1):

$$DoR = \frac{A - D}{1 + \left(\frac{t}{C}\right)^B} + D \quad (1)$$

where DoR presents the reaction degree, t the hydration time in days, A the minimum reaction degree (set to 0), B the maximum steepness of the curve, C the inflection point and D the maximum reaction degree (set to 100) [38,39].

Second, the changes in phase volumes during the hydration of BYF-B and BYF-Y clinkers were modelled within the temperature range of 0–85 °C. The phase compositions of the clinkers and gypsum, determined by X-ray powder diffraction, were utilised as input data. For ye'elimite, ferrite, periclase and mayenite reaction degrees of 100% were considered. For belite a reaction degree depending on temperature was used, which was inter- and extrapolated from a linear fit of the dissolution degrees at 5, 20, 40 and 60 °C after 150 days as obtained by X-ray powder diffraction. Anhydrite, gypsum, arcanite and aphthitalite were all assumed to react fully, while γ-dicalcium silicate, gehlenite and perovskite were considered as inert phases [40].

A water-to-cement ratio of 0.5 was applied in the calculations, which corresponds to the value used in the experiments.

According to the results of thermodynamic modelling, the porosities of the samples were calculated according to the equation (Eq. 2):

$$P = \frac{V_{\text{unhydrated cement, t=0}} + V_{\text{hydrates, t=0}} + V_{\text{pore solution, t=0}} - V_{\text{hydrates, t}} - V_{\text{unhydrated cement, t}}}{V_{\text{unhydrated cement, t=0}} + V_{\text{hydrates, t=0}} + V_{\text{pore solution, t=0}}} \times 100 \quad (2)$$

where P is the porosity (%), V the volume (cm^3), t = 0 the time at the beginning of hydration and t is time [41].

3. Results and discussion

3.1. Isothermal calorimetry

The influence of temperature on the hydration heat flow is shown in Fig. 1a (BYF-B) and 1b (BYF-Y). The initial peak, which can be attributed to the wetting and first hydration reactions [18,23,42,43], cannot be assessed due to external mixing.

The induction period, which occurs during a slow dissolution of the clinker phases and subsequent slow formation of hydrates [17,42–44], is prolonged at lower temperatures. Especially at 5 °C, the induction period is very long - about 11 h for BYF-B and 15 h for BYF-Y. A longer induction period at lower temperatures has also been observed by other authors [21,45]. At 20 °C, the induction period lasts until approximately 1.6 h in BYF-B and 1.5 h in BYF-Y. The samples cured at elevated temperatures have very short induction periods, around 20 min at 40 °C and 60 °C for both cements.

The maximum heat flow released during hydration increases with increasing temperature. At higher temperatures the reactions are faster and thus show significantly higher rates of heat release, indicating that increasing the curing temperature accelerates the hydration kinetics [17,20,22,46,47]. At 5 °C, the reaction is very slow, leading to a significantly lower rate of heat liberation compared to ambient and elevated temperatures.

At 5 °C, only a very broad first peak is seen in BYF-B, starting after around 11 h of hydration, which can – as also for all other samples – be attributed to the dissolution of ye'elimite and gypsum and the early precipitation of ettringite and aluminium hydroxide [17,18,42,48,49], with a small additional maximum occurring after 27.5 h, which can be attributed to the precipitation of monosulfate and/or ettringite [40,42,49]. At 20 °C, the first heat evolution peak occurs after 3.5 h of hydration, followed by a second peak after 5.2 h. At 40 °C the first peak occurs after 0.8 h and the second after 1.5 h, while at 60 °C they occur even earlier - after 0.6 and 1.2 h, respectively.

In BYF-Y, at 5 °C, the first peak occurs between 15 and 37.5 h of hydration, with no clear maximum, while a second maximum is visible after 40 h. At all other temperatures, the first peaks occur at a similar time to BYF-B, while the second peaks are shifted to later times in comparison to BYF-B, appearing after 8.2, 2.7 and 1.4 h at 20 °C, 40 °C and 60 °C, respectively. This is related to the fact that in BYF-Y more

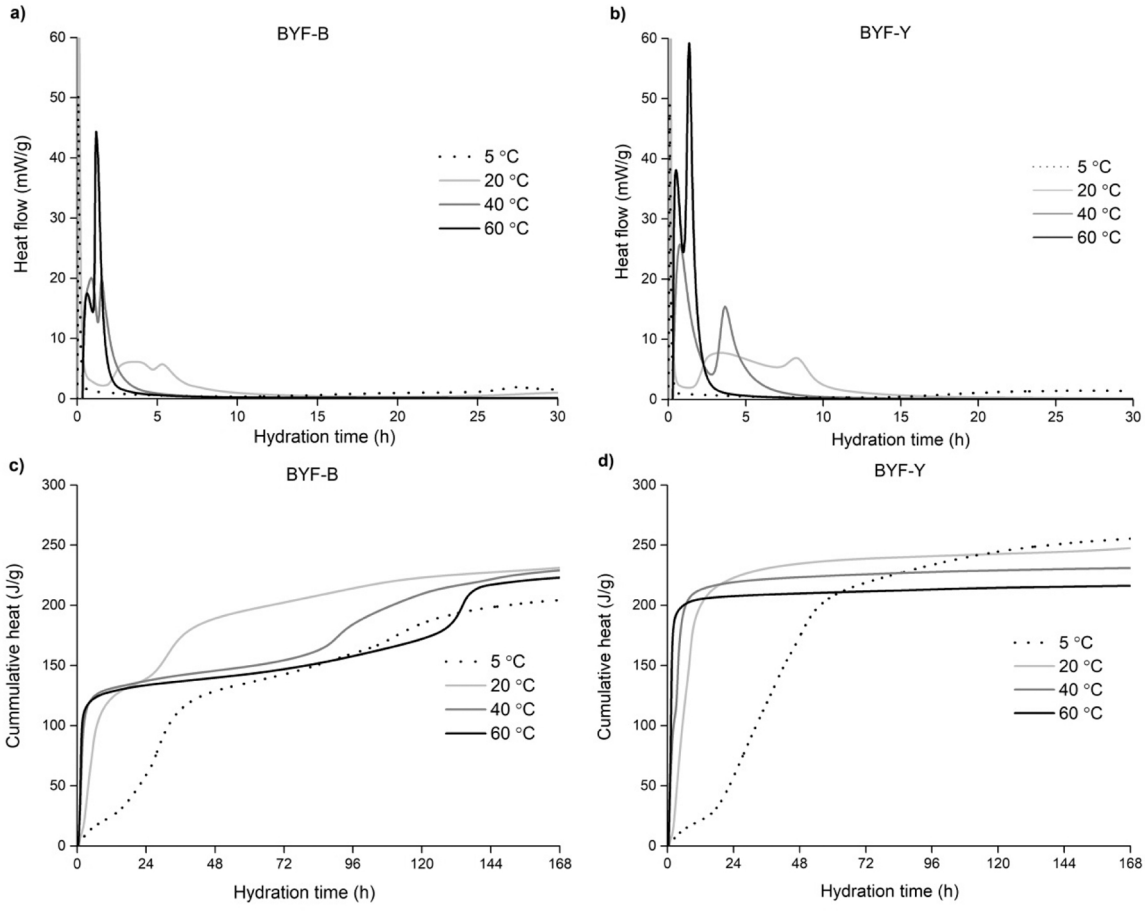

Fig. 1. Hydration heat flow (a, b) and development of cumulative heat of hydration (c, d) of BYF-B and BYF-Y cements, respectively, at different curing temperatures. Both the heat flow and the cumulative heat are normalised to the weight of the cement. Data at 20 °C were taken from [26].

ettringite forms than monosulfate due to the higher content of ye'elimite in clinker BYF-Y compared to BYF-B (see Table 2). As indicated, at elevated temperatures the reactions occur at an earlier time. However, it can be seen that raising the temperature from 40° to 60°C does not show a significant difference in terms of heat release in the case of BYF-B in contrast to BYF-Y.

The development of cumulative heat is displayed in Fig. 1c and d. The results show that after 7 days of hydration, the cumulative heat for cement mixture BYF-B decreases with increasing temperature from 20 to 60 ºC. After 7 days the cumulative heat is lower at 5 ºC than at other temperatures, indicating very slow and long-term hydration. However, on the one hand, at 40 and 60 °C the very early heat of hydration might not be entirely captured as we had to discard the first 30 min of the heat flow due to the external mixing procedure. On the other hand, like in Portland cement, after long hydration times and low temperatures often higher hydration degrees are reached than at high temperatures, where fast hydration leads to dense shells of hydrates around the clinker grains [1]. In the case of low temperatures dissolution is slow, and the ions have time to distribute in the matrix and to precipitate in the pore space.

For BYF-Y the cumulative heat after 7 days decreases when the temperature is increased from 5 to 60 ºC. The long-term reaction slows down faster when the temperature is increased in both cement mixtures, which was also observed by Chitvoranund [22].

3.2. Dissolution of clinker phases and gypsum

Figs. 2 and 3 plot the XRD patterns of BYF-B and BYF-Y at the different curing temperatures after 1 and 150 days of hydration, while the patterns related to the curing times of 7 and 28 days are available in Figs. S1 and S2 in the Electronic Supplementary Material (ESM). Figs. 4 and 5 plot the phase contents of the main anhydrous phases (belite, ye'elimite, ferrite and gypsum) at different curing temperatures for BYF-B and BYF-Y, respectively. Phase quantifications of the cements BYF-B and BYF-Y cured at 5, 20, 40 and 60 ºC at various hydration times are presented in Figs. 6 and 7.

As the temperature is increased, the dissolution of anhydrous clinker phases is accelerated, as has been observed previously in both Portland cements [1,3,10,46] and ye'elimite-based cements [16,18,21]. Ye'elimite reacts very rapidly and at ambient and elevated temperatures is almost fully consumed during the first day of hydration.

At 5 ºC, the consumption of ye'elimite and gypsum is significantly slowed down at early ages in comparison to the other temperatures. At 1 day, the reaction degrees of ye'elimite are around 60% and 55% for BYF-B and BYF-Y, respectively (Figs. 5 and 6). Gypsum is almost fully reacted after 1 day in BYF-B, while only approximately 60% have reacted in BYF-Y over the same period of time, as the amount of added gypsum in BYF-Y is almost twice the amount in BYF-B (Fig. 5). TGA results confirm the presence of gypsum at a curing temperature of 5 ºC at 1 day of hydration (Fig. 8). The results indirectly confirm X-ray powder diffraction results, which show that at 1 day the hydration degree of clinker phases is the lowest at 5 ºC, as a lower quantity of bound water is identified compared to other temperatures.

The reaction kinetics of belite is slower compared to ye'elimite and gets faster with higher temperatures. In the first 24 h, there is some reaction of belite at all temperatures. After 1 day, the hydration degree of BYF-B reaches around 35% at 5, 20 and 40 ºC, and almost 50% at 60 ºC. For BYF-B hydration of belite grows substantially beyond 7 days of hydration and is promoted at elevated temperatures. After 150 days nearly 90% of belite is hydrated at 60 ºC in comparison to 5 ºC, where a hydration degree of approximately 50% is reached. Similar hydration degrees of belite at 5 ºC and 60 ºC were also reported in [22] after 180 days, although only little reaction was observed until 90 days. For BYF-Y the hydration degree of belite after 1 day is around 40% for all temperatures. At 60 °C, the hydration of belite significantly increases between 7 and 28 days of hydration, while at lower temperatures this increase takes place beyond 28 days. After 150 days the hydration degree of belite is around 80% at 60 °C and approximately 60% at 5 °C.

In the BYF-B cement mixture, unreacted ferrite is only present at 1 day of hydration and not detected after 7 days, suggesting it is already dissolved. In line with previous findings [46,47], the hydration degree of

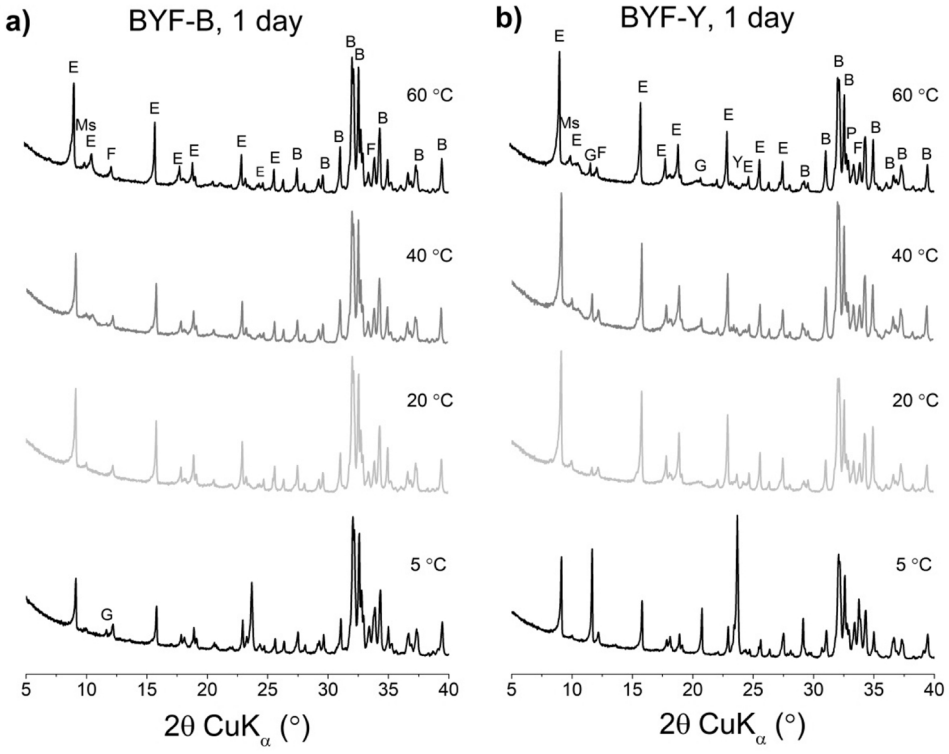

Fig. 2. X−ray diffraction patterns of BYF-B (a) and BYF-Y (b) at different curing temperatures at 1 day of hydration. B = belite, E = ettringite, F = ferrite, G = gypsum, Ms = monosulfate P = perovskite, Y = ye'elimite. Data at 20 ºC were taken from [26].

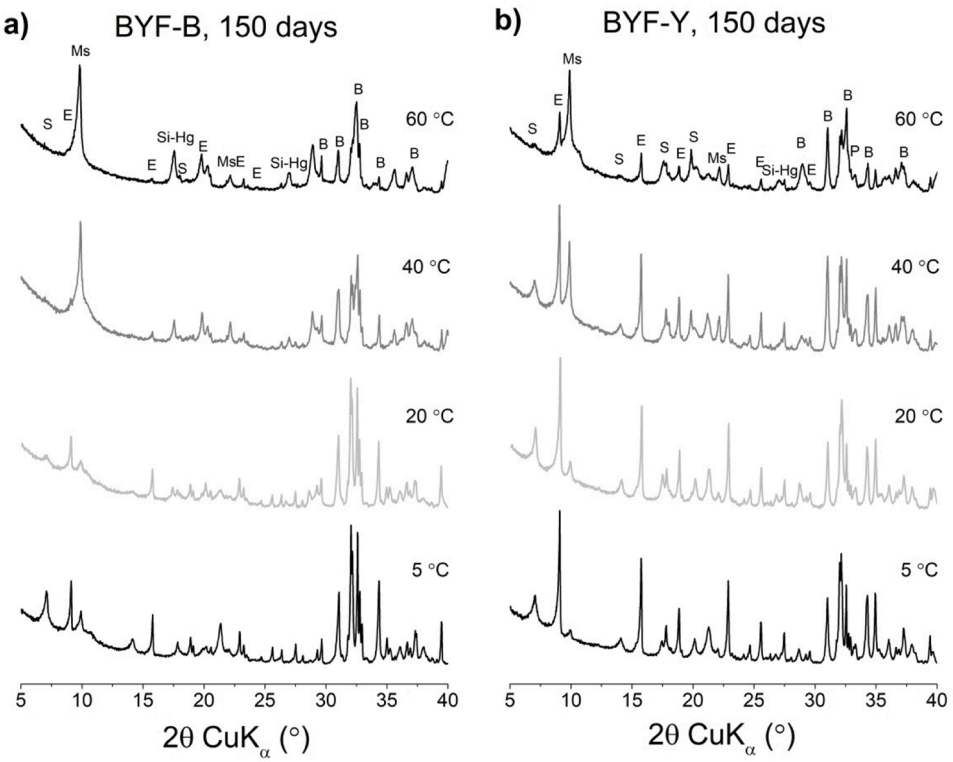

Fig. 3. X−ray diffraction patterns of BYF-B (a) and BYF-Y (b) at different curing temperatures at 150 days of hydration. B = belite, E = ettringite, Ms = monosulfate, P = perovskite, S = strätlingite, Si-Hg = siliceous hydrogarnet. Data at 20 °C were taken from [26].

ferrite at 1 day does not change significantly with temperature, reaching around 60% at 20, 40 and 60 °C, and a somewhat lower value at 5 °C (50%). In BYF-Y ferrite is consumed slower than in BYF-B; it is still detected at 7 days of hydration. At 5 °C, the hydration degree is approximately 54% after 1 day, while at the increased temperature it is slightly higher (60%).

Whilst mayenite, arcanite and aphthitalite could not be detected after 1 day of hydration, γ-C_2S, perovskite and gehlenite were all found to be non-reactive.

3.3. Development of the hydration products

XRD results reveal the presence of ettringite, monosulfate, strätlingite and siliceous hydrogarnet as crystalline hydration products in the hydrated samples (Figs. 6, 7). Aluminium hydroxide, which also forms upon the hydration of ye'elimite-based cements, is generally X-ray amorphous but can be identified by thermogravimetric analyses, especially at early ages (see Figs. 8, 9 and Fig. S3 in the Electronic Supplementary Material (ESM)). C−S−H as a further potential hydration product is difficult to detect, but can potentially be identified by a very broad signal in both XRD and by TGA, and more clearly by using SEM/BSE with EDX. In general, it can be observed that the type of hydration products does not change, but their amounts change when the curing temperature is altered in both BYF-B and BYF-Y [1,16,21].

As mentioned above, the early hydration of ye'elimite in the presence of gypsum is slower at 5 °C than at elevated temperatures, which directly results in a lower amount of precipitated ettringite after 1 day of hydration in comparison to increased temperatures. However, with ongoing hydration between 7 and 150 days less ettringite and slightly more monosulfate are present when the temperature is increased, which is in accordance with previous studies [1,2,16,17,21,46,47,50]. Ettringite, together with aluminium hydroxide, precipitates with the hydration of ye'elimite and gypsum according to Eq. 3, while monosulfate forms after sulphate depletion according to Eq. 4 [23,48,51–56]:

$$C4A_3\overline{S} + 2C\overline{S}H_x + (38-2x)H \rightarrow C_6A\overline{S}_3H_{32} + 2AH_3 (x = 0, 0.52) \quad (3)$$

$$C_4A_3\overline{S} + 18\ H \rightarrow C_4A\overline{S}H_{12} + 2AH_3 \quad (4)$$

With increasing temperature, the solubility of ettringite is higher which promotes monosulfate formation and leads to an increase of sulphate concentration in the pore solution [1,19,21,50]. At 5 °C, the hydration of ye'elimite generates initial low ettringite amounts, but later much more, especially after 7 days, while only a small amount of monosulfate is formed in comparison to higher temperatures [21]. In addition, with time the amount of ettringite decreases at the expense of the monosulfate. The results of TGA analyses are in agreement with X-ray powder diffraction results, confirming that in the long-term less ettringite is generated at higher temperatures [21]. As can be seen from Figs. 8 and 9, in both BYF-B and BYF-Y, the main weight loss measured at 120 °C, assigned to ettringite [21,44,52,57], decreases with hydration time. In both mixtures, its amount decreases with higher temperatures from 7 days onwards. Furthermore, the results indicate, as expected, that much more ettringite is present in the ye'elimite-rich BYF-Y compared to BYF-B.

Potentially, C−S−H with a broad weight loss area between 50 and 250 °C [34] could also be present, but this is difficult to clearly assess under the intense weight loss caused by the decomposition of ettringite. In addition, aluminium hydroxide forms due to the hydration of ye'elimite during the first day of hydration, but seems to be already largely consumed after 1 day and 28 days for BYF-B and BYF-Y, respectively, due to its reaction with belite to form strätlingite according to Eq. 5 [52,58,59]:

$$C_2S + AH_3 + 5\ H \rightarrow C_2ASH_8 \quad (5)$$

Aluminium hydroxide loses its bound water and exhibits an endothermic peak at around 250–280 °C [21,44,52,57], however, it was not identified by X-ray diffraction due to its amorphous nature [40,60]. TGA

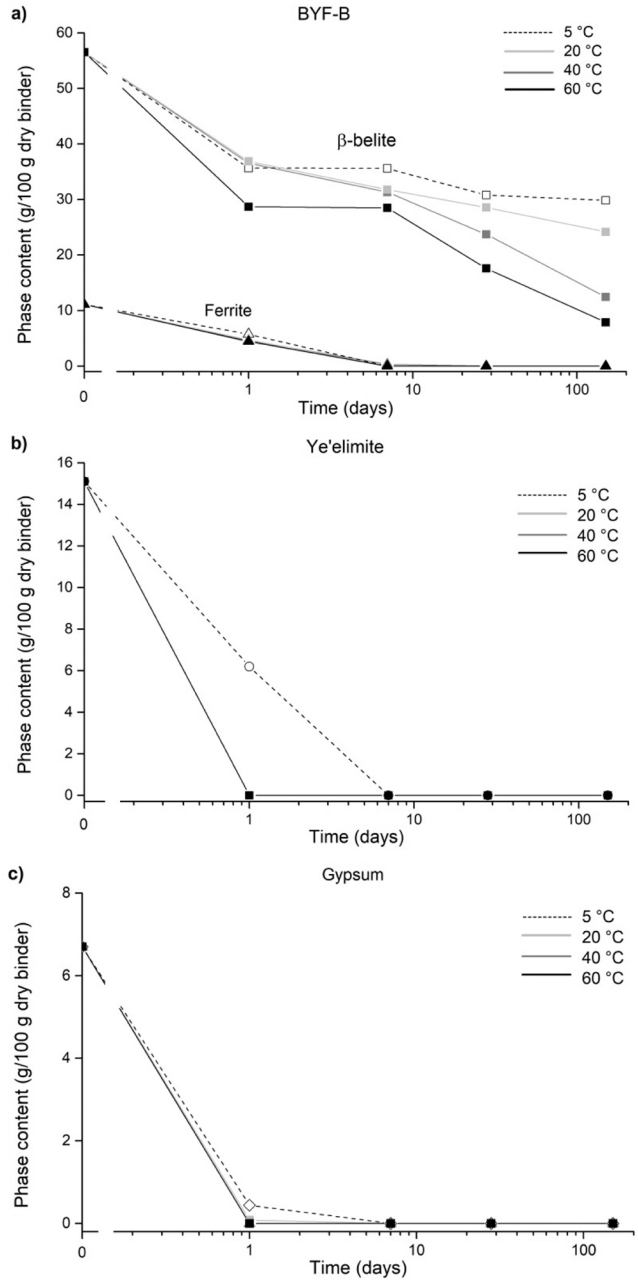

Fig. 4. Phase contents of β-belite and ferrite (a), ye'elimite (b) and gypsum (c) in the BYF-B cement mixture obtained by quantitative X-ray diffraction. The estimated relative errors are ± 5%. Data at 20 °C were taken from [26].

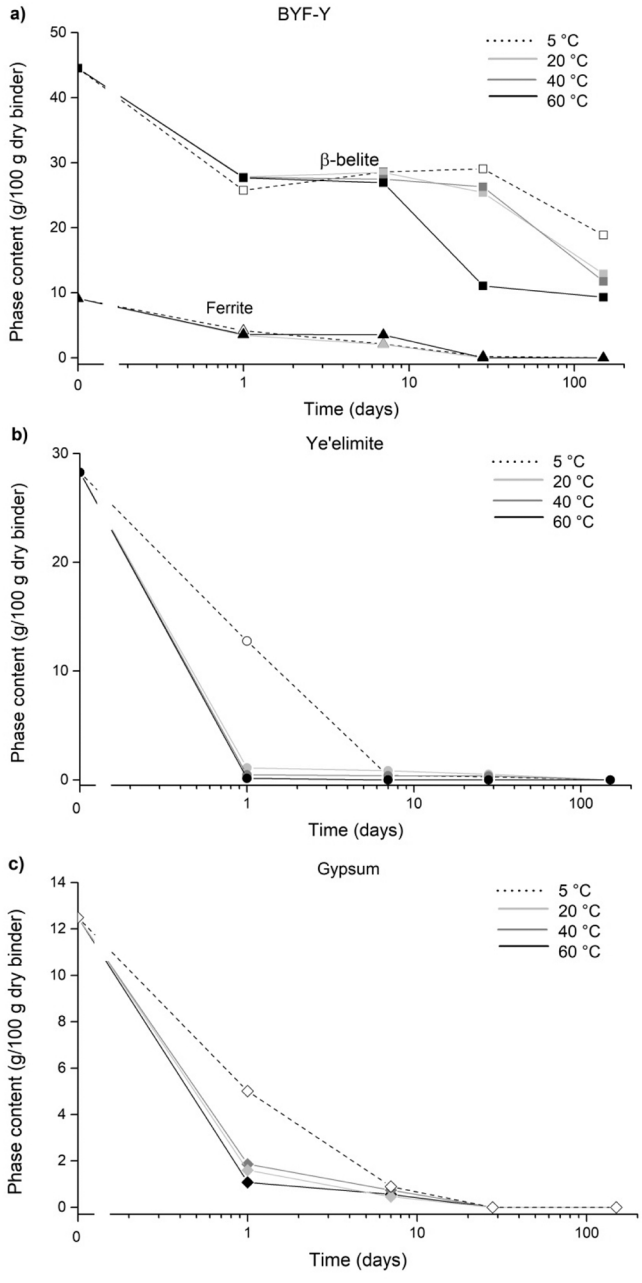

Fig. 5. Phase contents of β-belite and ferrite (a), ye'elimite (b) and gypsum (c) in the BYF-Y cement mixture obtained by quantitative X-ray diffraction. The estimated relative errors are ± 5%. Data at 20 °C were taken from [26].

shows that more aluminium hydroxide forms initially at elevated temperatures, indicating aluminium hydroxide formation is promoted at high temperatures, as reported elsewhere [16,17,21]. More aluminium hydroxide is observed in BYF-Y than in BYF-B due to the lower belite content of the former.

In BYF-B strätlingite is identified after 7 days of hydration, while in BYF-Y is only identified at 150 days at 5 °C and after 28 days at ambient and elevated temperatures, as less belite is present in that blend and as belite hydration is slower at low temperatures. However, a part of strätlingite might be amorphous or poorly crystalline, and thus difficult to be detected by XRD. The amount of strätlingite decreases with increasing temperatures significantly after 28 days in BYF-B and after 150 days in BYF-Y, when the formation of siliceous hydrogarnet is observed. The latter phase precipitates due to the hydration of ferrite [52], according to Eq. 6:

$$C_4AF + C_2ASH_8 + 5\,H \rightarrow 2\,C_3(A,F)SH_4 + AH_3 \quad (6)$$

At elevated temperatures, higher contents are observed especially at 60 °C as also confirmed by TGA data. When more belite hydrates, siliceous hydrogarnet and possibly also C–S–H form on the expenses of strätlingite as suggested by the modelling (see Section 3.5). This increased amount of siliceous hydrogarnet at elevated temperatures is in agreement with other observations in Portland and calcium sulfoaluminate cements [2,16,48]. In a recent study by Chitvoranund [22]small amounts of Si-hydrogarnet were observed in belite-ye'elimite system, however only at 60 °C, as no significant content of ferrite was present in cement clinker. The precipitation of siliceous hydrogarnet is favoured by increased temperatures due to kinetic reasons [16,61], some amount is detected in this study also at 20 °C and 40 °C after 28 days of hydration

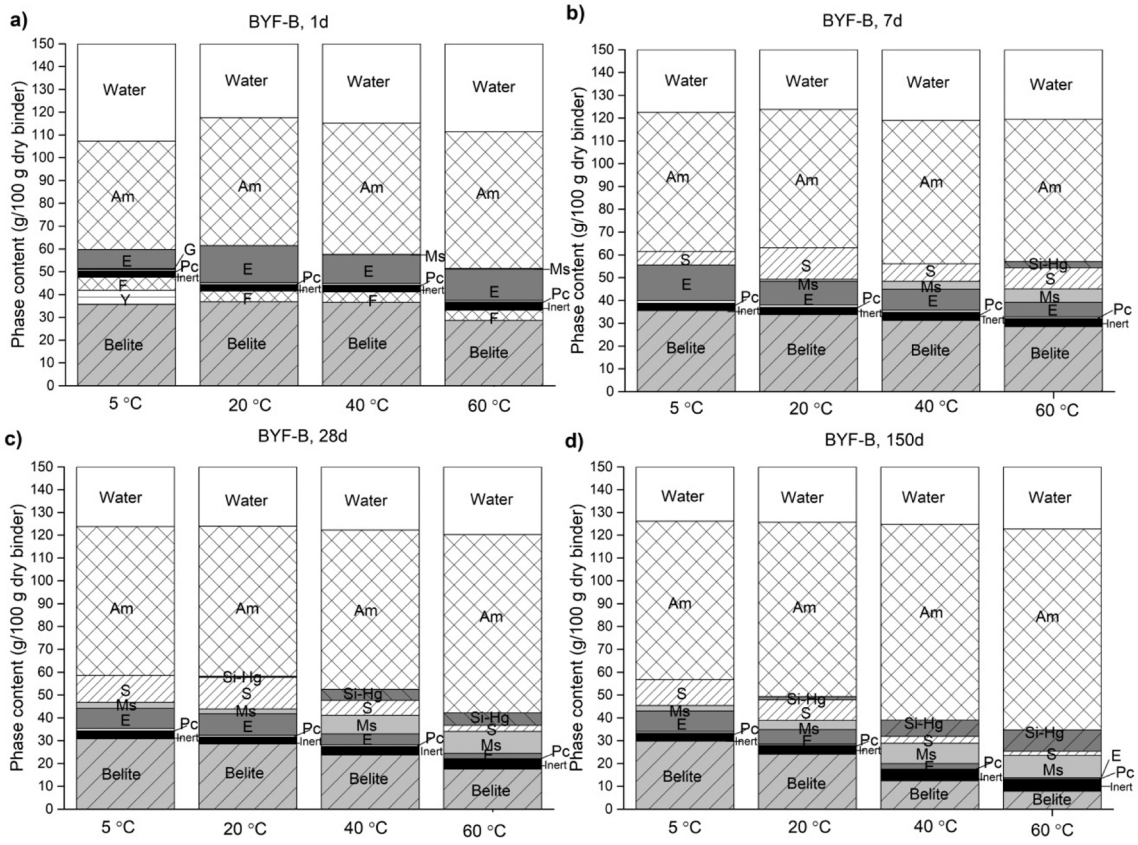

Fig. 6. Comparison of the phase assemblages of cement mixture BYF-B at different temperatures as determined by quantitative X-ray diffraction. Am = amorphous, E = ettringite, F = ferrite, G = gypsum, Ms = monosulfate, Pc = periclase, S = strätlingite, Si-Hg = siliceous hydrogarnet, Y = ye'elimite. Data at 20 ºC were taken from [26].

in BYF-B and after 150 days in BYF-Y.

The bound water contents as derived from TGA are shown in Fig. 10, where mainly the different amounts of ettringite are reflected in the amounts of bound water, as ettringite contains the most bound water among the hydrates, while the ettringite peak in TGA overlaps with C–S–H's. Thus bound water content is higher for the ye'elimite-rich cement compared to the belite-rich cement, as more ettringite is formed in this cement. While after 1 day of hydration, the amount of bound water is significantly lower at 5 °C in comparison to higher temperatures, both BYF-B and BYF-Y reach comparable bound water contents after 150 days with the exception of 60 °C, in agreement with the observed amounts of ettringite.

3.4. Microstructural characterisation of the hydrate phases

Figs. 11–14 show SEM/BSE images of polished sections of the BYF-B and BYF-Y cement at 150 days of hydration at different temperatures. All samples have a dense matrix with low porosity. At elevated temperatures (40 and 60 °C), the microstructure is less dense and the hydration products are more heterogeneously distributed in comparison to lower temperatures, where individual hydration products are harder to detect. Previous studies on Portland cements and calcium sulfoaluminate cements have shown that the heterogeneity of cement pastes is higher at increased temperatures due to faster hydration [1,16,62]. Grains of anhydrous clinker are present at 5 °C, as shown in Fig. 12. At elevated temperatures (Figs. 12–14), smaller and less anhydrous grains are present in comparison to 5 °C, confirming a higher degree of hydration as observed by XRD. Similar findings were already reported in [16]. The matrix consists of ettringite, AFm phases (monosulfate, strätlingite, hydrogarnet) and C–S–H as identified by EDS analysis. Ettringite is far more prominent in the BYF-Y mixture than in BYF-B. In addition, it is observed that its amount is lower at elevated temperatures, in agreement with XRD and TGA observations and thermodynamic modelling. Monosulfate and strätlingite are difficult to differentiate in BSE images; monosulfate usually appears as platelets, strätlingite in elongated shapes. C–S–H is finely distributed in the interstitial free space between ettringite and monosulfate and not around the calcium silicate clinker phases (in this case only belite) in contrast to Portland cement [22].

The results of EDS analyses are shown as atomic ratio plots (Figs. 15 and 16) due to the small size of the hydrate phases and the interaction volume of electrons with a sample, which causes that X-rays to consist of a mixed signal of different phases [63].

The results show that the phase composition of the hydrate assemblage changes with temperature, as well as with the compositions of the cement clinker (Fig. 15). At 5 °C, EDS analyses indicate the presence of ettringite and monosulfate in BYF-B at 150 days, as the EDS points are located in the area between the composition of these phases. Furthermore, some strätlingite and C–S–H are detected. This is in agreement with XRD and TGA results, which indicate the formation of ettringite, monosulfate and strätlingite; C–S–H however is not possible to be clearly identified with those methods. Similarly, ettringite and monosulfate are observed at 20 °C, however, it can be seen that more data points are located towards monosulfate than ettringite in comparison to 5 °C. Data points between ettringite and strätlingite confirm the formation of strätlingite. Also, some data points between monosulfate and C–S–H are occurring. At 40 and 60 °C only a small amount of data points is located towards ettringite, while the main share is directed towards monosulfate and C–S–H. In addition, it can be seen that less or almost no strätlingite is present, as only a few points are close to this

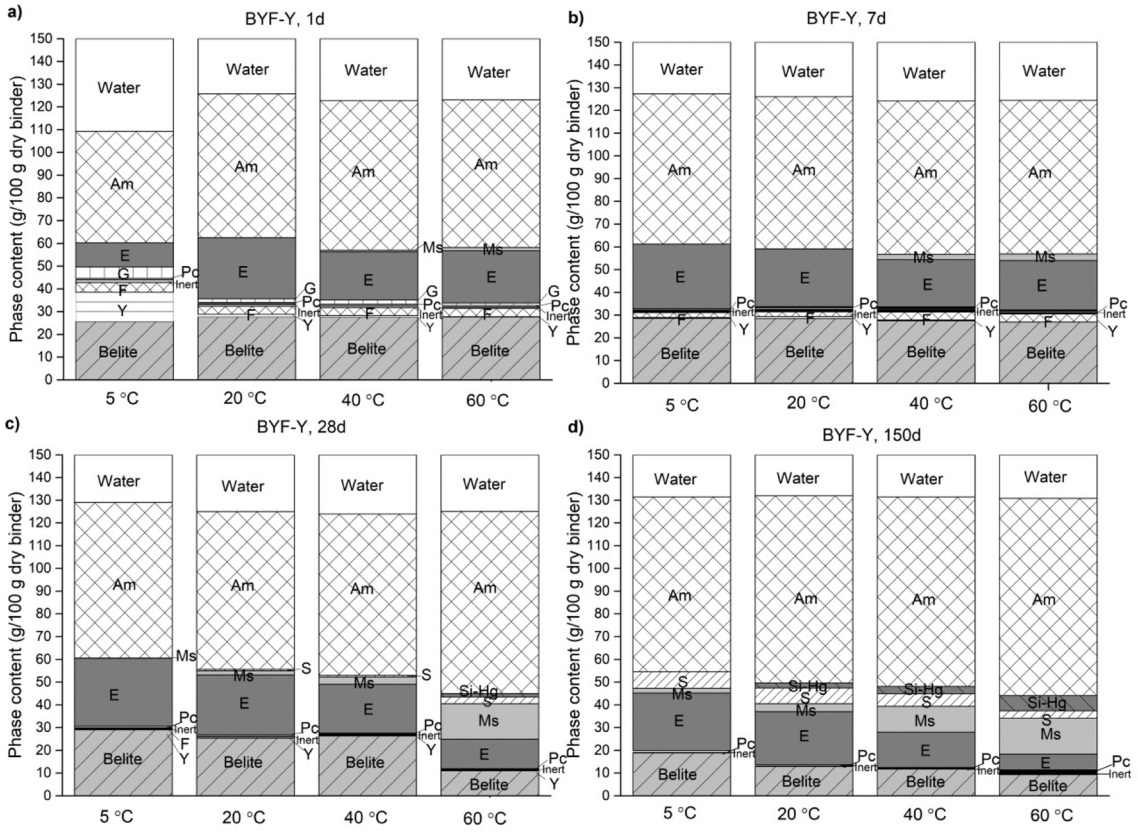

Fig. 7. Comparison of the phase assemblages of cement mixture BYF-Y at different temperatures as determined by quantitative X-ray diffraction. Am = amorphous, E = ettringite, F = ferrite, G = gypsum, Ms = monosulfate, Pc = periclase, S = strätlingite, Si-Hg = siliceous hydrogarnet, Y = ye'elimite. Data at 20 °C were taken from [26].

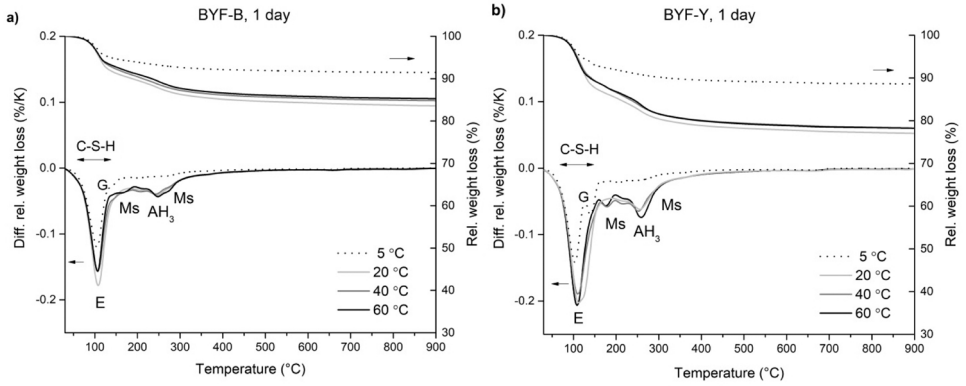

Fig. 8. Thermogravimetric analyses of cement pastes BYF-B (a) and BYF-Y (b) at different temperatures at 1 day of hydration. AH_3 = aluminium hydroxide, C-S-H = calcium silicate hydrate, E = ettringite, G = gypsum, Ms = monosulfate. Data at 20 °C were taken from [26].

phase, which corresponds to XRD and TGA results.

In contrast to cement BYF-B, significantly more data points are directed towards the composition of ettringite for BYF-Y. Monosulfate is indicated as well, and more data points related to this phase are present at elevated temperatures. The trend towards strätlingite at elevated temperatures is more pronounced in BYF-Y than in BYF-B. A low content of C–S–H might also be present in BYF-Y as data points are visible in the area near the composition of C–S–H. Siliceous hydrogarnet could be present according to EDS in both cements.

Fig. 16 plots graphs of different atomic ratios of samples cured at 20 °C at 1, 7 28 and 150 days of hydration. EDS analyses confirm the presence of ettringite as the main hydration product at 1 day of hydration in BYF-B, as detected also with X-ray powder diffraction. At 7 days of hydration, a small amount of data points is located towards monosulfate, while a majority of data points are also located towards strätlingite. After 28 and 150 days of hydration and in addition to the presence of strätlingite, a much more visible trend between the compositions of monosulfate and C–S–H is occurring.

For BYF-Y, the data points at 1 day are much more dispersed, probably due to the presence of unreacted ye'elimite and gypsum. At all hydration times, the data points are directed mainly towards ettringite. A trend towards strätlingite is observed at 150 days. A small amount of C–S–H seems to be indicated at all hydration times as a few points also are close to this phase.

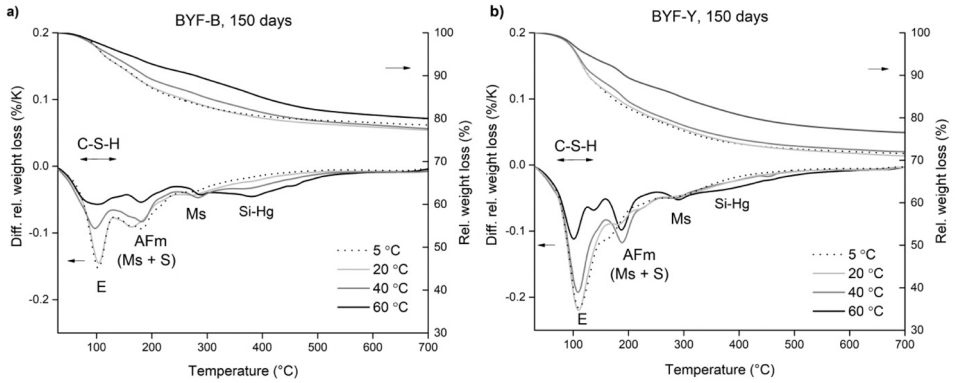

Fig. 9. Thermogravimetric analyses of cement pastes BYF-B (a) and BYF-Y (b) at different temperatures at 150 days of hydration. C-S-H = calcium silicate hydrate, E = ettringite, Ms = monosulfate, S = strätlingite, Si-Hg = siliceous hydrogarnet. Data at 20 ºC were taken from [26].

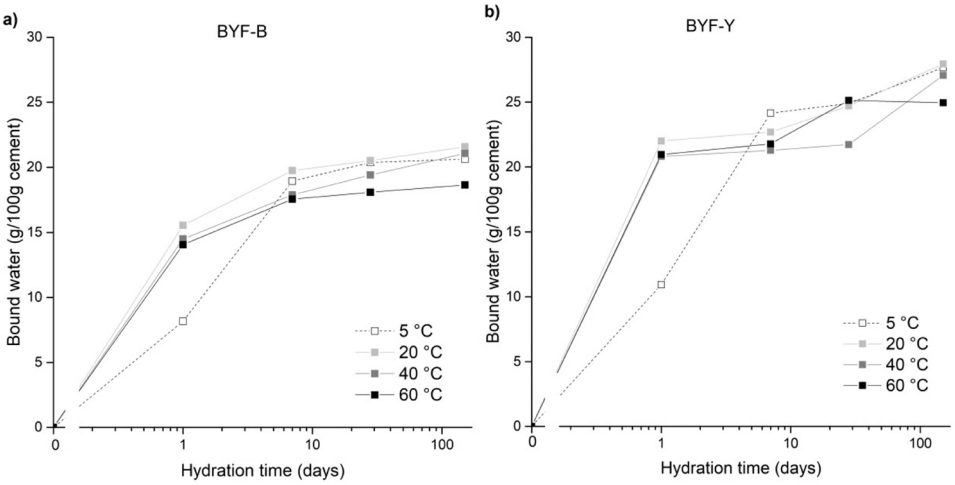

Fig. 10. Bound water as determined by thermogravimetric analyses up to 150 days of hydration (normalised to anhydrous cement) for different temperatures plotted against curing time. Data at 20 ºC were taken from [26].

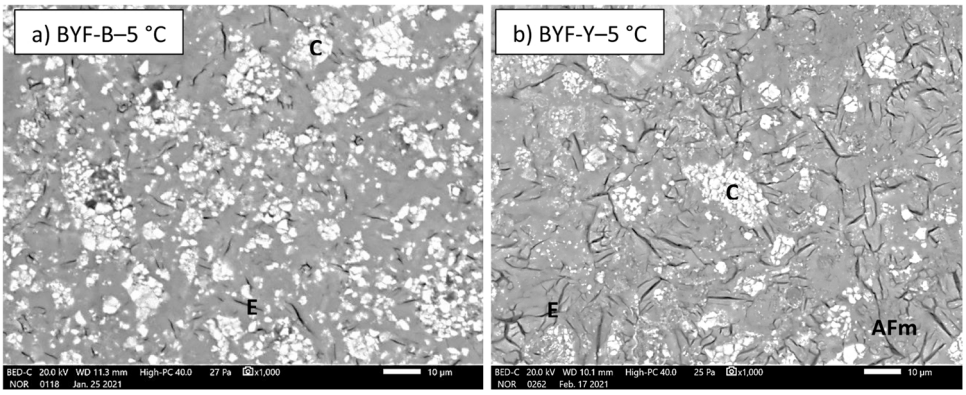

Fig. 11. SEM/BSE images of the BYF-B (a) and BYF-Y (b) cements cured at 5 °C at 150 days of hydration, showing the residual clinker phases and hydration products that precipitated. C = unhydrated clinker, E = ettringite, AFm = monosulfate, strätlingite.

3.5. Thermodynamic modelling of phase development with time and temperature

Figs. 17 and 18 show the modelled hydrate assemblages of BYF-B and BYF-Y cements with ongoing hydration at 5, 20, 40 and 60 °C. In both investigated systems (BYF-B, BYF-Y) and at all temperatures, the calculated stable hydrate phases are ettringite, monosulfate, strätlingite, C–S–H, siliceous hydrogarnet, and hydrotalcite. Aluminium hydroxide is formed only in BYF-Y cement at 20, 40 and 60 °C, and at early times traces of portlandite and brucite, which were not observed experimentally; their occurrence might also be an artefact from the different reaction degrees fitted for ye'elimite and belite. In general, the differences in the amounts of hydrate phases between various temperatures are predicted based on the faster kinetics with increasing temperature in agreement with the experimental data. Ettringite is the main hydration product predicted at early ages, as a result of the fast hydration of

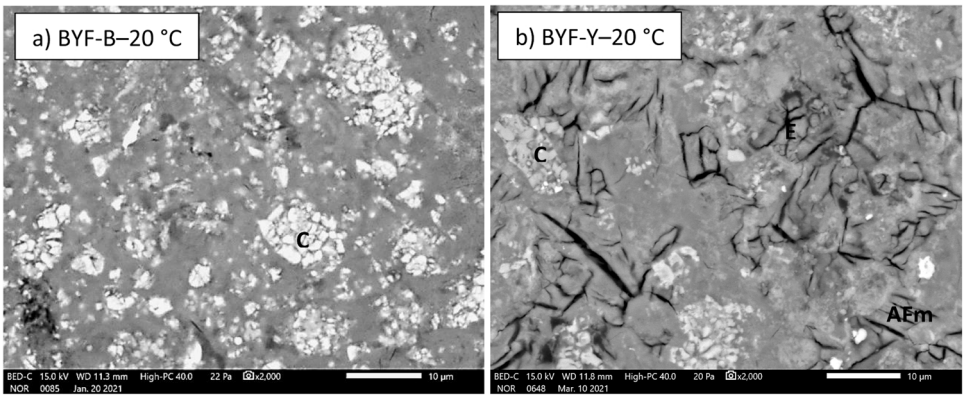

Fig. 12. SEM/BSE images of BYF-B (a) and BYF-Y (b) cements cured at 20 °C at 150 days of hydration, showing the residual clinker phases and hydration products that precipitated. C = unhydrated clinker, AFm = monosulfate, strätlingite.

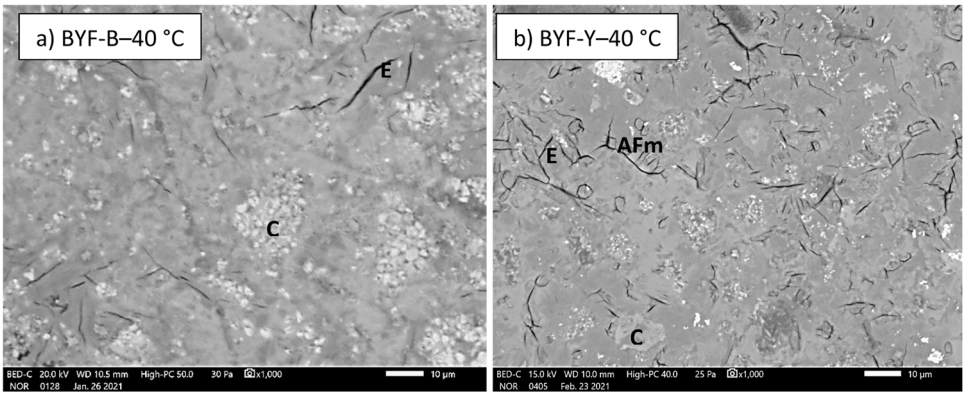

Fig. 13. SEM/BSE images of BYF-B (a) and BYF-Y (b) cements cured at 40 °C at 150 days of hydration, showing the residual clinker phases and hydration products that precipitated. C = unhydrated clinker, E = ettringite, AFm = monosulfate, strätlingite.

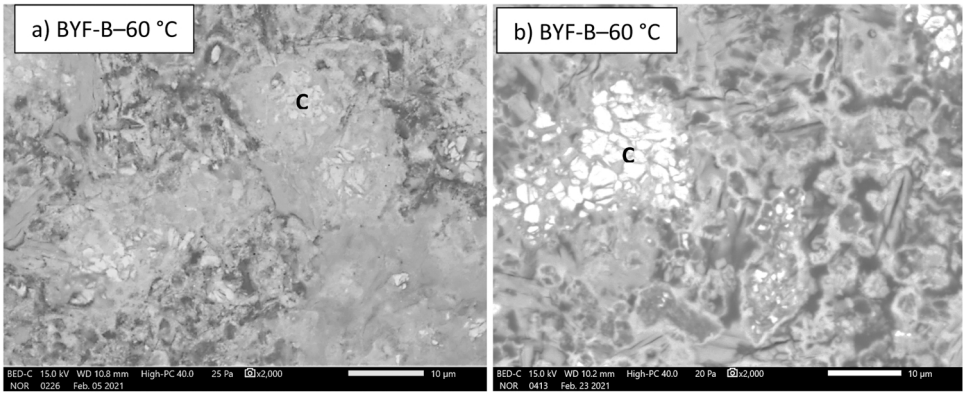

Fig. 14. SEM/BSE images of BYF-B (a) and BYF-Y (b) cements cured at 60 °C at 150 days of hydration, showing the residual clinker phases and hydration products that precipitated. C = unhydrated clinker.

ye'elimite and gypsum. When gypsum is depleted, monosulfate forms at the expense of ettringite. With increasing temperature higher amount of monosulfate is predicted, while there is less ettringite. In BYF-Y significantly more ettringite and less monosulfate are calculated in comparison to BYF-B. Furthermore, a higher amount of ettringite in BYF-Y results in a lower amount of pore solution, as ettringite consumes more water. The modelling indicates the presence of strätlingite, C–S–H and siliceous hydrogarnet in both cements, which agrees with XRD, TGA and EDX data. More strätlingite is predicted by thermodynamic modelling than determined experimentally, suggesting that strätlingite is also present in an X-ray amorphous form as also reported elsewhere [22]. The models predict a higher quantity of C–S–H at elevated temperatures as more belite reacts.

3.6. Compressive strength

The results of the compressive strength measurements of cements BYF-B and BYF-Y at different temperatures are shown in Fig. 19.

Both cements exhibit rapid early strength development at 20, 40 and 60 °C, as a result of the fast reaction of ye'elimite and gypsum with water and consequently the formation of ettringite, which significantly contributes to early strength [1,2,22,64,65]. Strength development is

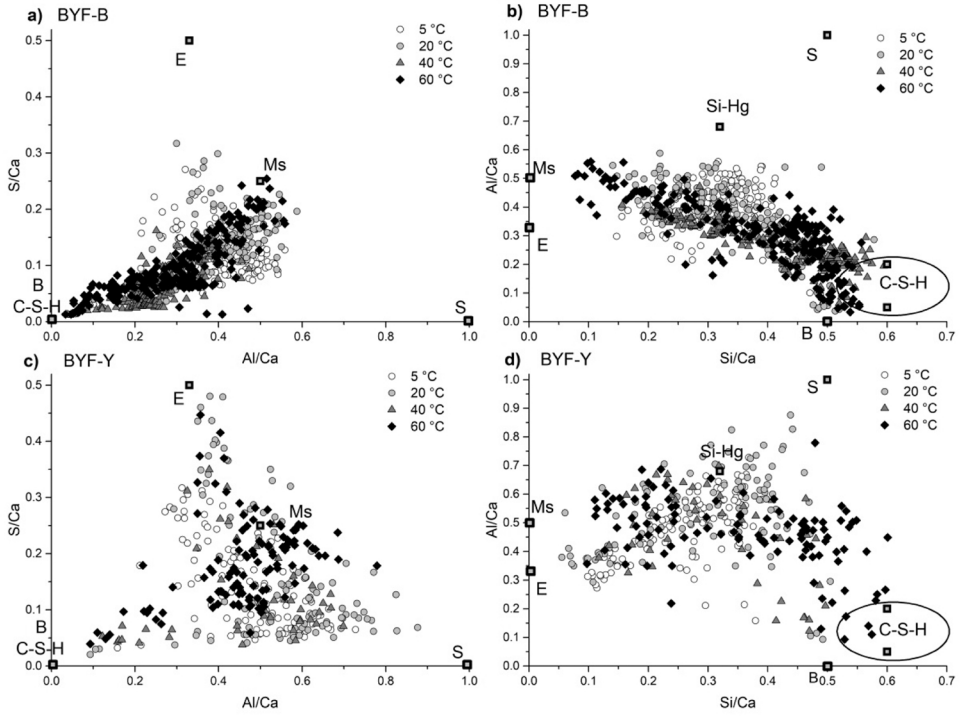

Fig. 15. EDS analyses of BYF-B (a and b) and BYF-Y pastes (c and d) at 150 days of hydration at different curing temperatures. Grey squares = pure phases: B = belite, C–S–H = calcium silicate hydrate, E = ettringite, Ms = monosulfate, S = strätlingite, Si-Hg = siliceous hydrogarnet.

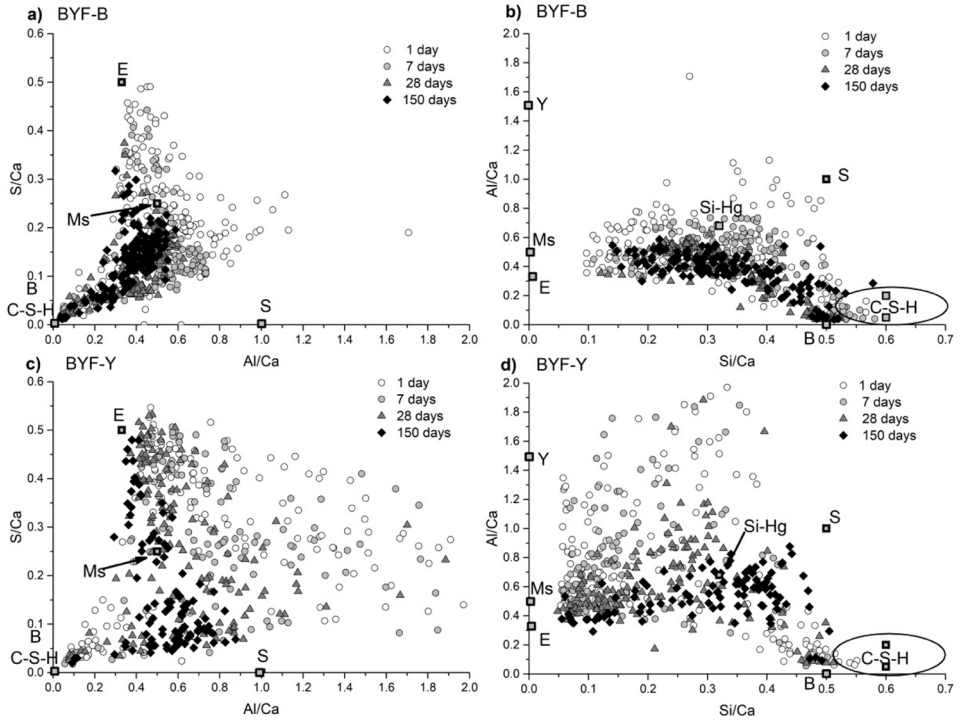

Fig. 16. EDS analyses of BYF-B (a and b) and BYF-Y pastes (b and c) at 20 °C at different curing times. Grey squares = pure phases: B = belite, C–S–H = calcium silicate hydrate, E = ettringite, Ms = monosulfate, S = strätlingite, Si-Hg = siliceous hydrogarnet, Y = ye'elimite.

rather slow at 5 °C for both cements in agreement with other studies [1,21,22,45]. X-ray diffraction and thermogravimetry results show that in BYF-B gypsum is already consumed within the initial 24 h of hydration at 20, 40 and 60 ºC, while a small amount stays unreacted at 5 ºC. In BYF-Y a much higher amount of unreacted gypsum is still present at 5 ºC, which results in lower strength after 1 day of hydration compared to BYF-B.

The results show that in both cements the compressive strength at late ages increases with increasing temperatures. For BYF-B the highest compressive strength after 150 days is reached at 60 ºC (38.3 MPa),

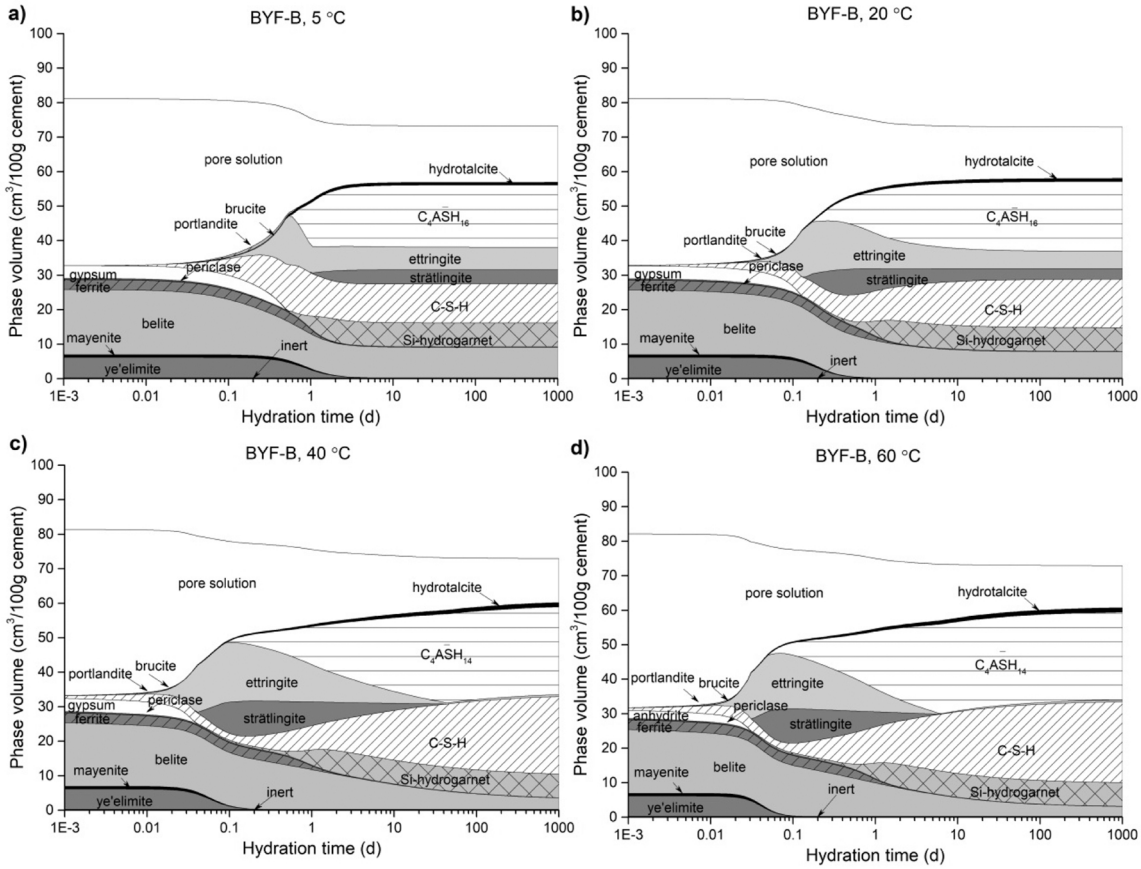

Fig. 17. Thermodynamic models of the phase assemblages as a function of hydration time at 5 °C (a), 20 °C (b), 40 °C (c) and 60 °C (d) for the BYF-B cement.

followed by 40 ºC (30.7 MPa) and 20 ºC (30.3 MPa), while at 5 ºC only 22.1 MPa are reached. For BYF-Y the values were 51.3 MPa, 49.3 MPa, 45.7 MPa and 38.2 MPa at 60, 40, 20 and 5 ºC, respectively. While studies on ordinary Portland cement and calcium sulfoaluminate cements report that compressive strength decreases at higher curing temperatures, previous studies on belite cements showed that compressive strength increases at elevated temperatures [46,66,67], as a result of an increased degree of belite hydration. In the case of the investigated cements, the increased hydration of belite at elevated temperatures, which takes place beyond 7 days of hydration, leads to the formation of additional, space-filling hydrates such as strätlingite, C–S–H and siliceous hydrogarnet, causing a strength increase at elevated temperatures.

Comparing cements BYF-B and BYF-Y it can be observed that BYF-Y develops a higher compressive strength than BYF-B, probably due to the higher ye'elimite content and the associated formation of more ettringite. However, at 5 ºC early compressive strength is lower in BYF-Y than in BYF-B due to the slow hydration of ye'elimite until 1 day at low temperatures.

Fig. 20a depicts the comparison between bound water as determined by TGA and measured compressive strength at investigated temperatures. With increasing bound water contents higher compressive strengths are found as a higher volume of hydrates is formed. Note, that a significant amount of water is bound even at (low) compressive strength at 5 °C. As expected, the compressive strength increases with decreasing porosity derived from thermodynamic modelling, as shown in Fig. 20b.

3.7. Thermodynamic modelling of the effect of temperature on the hydrate assemblage

The modelled phase composition of the cement paste BYF-B at late ages depending on temperature is plotted in Fig. 21a. The stable hydrate phases predicted in the whole temperature range between 0 and 85 ºC are siliceous hydrogarnet, C–S–H, monosulfate and hydrotalcite. Low amounts of ettringite are calculated to be present from 0 to 25 ºC. Traces of katoite are predicted to occur between 55 and 70 ºC, although in reality the additional aluminium might rather be bound C–S–H, which was not taken into account in the modelling. Above 70 ºC small amounts of portlandite are calculated as well as more belite reacts at higher temperatures. C–S–H and monosulfate are the most abundant phases, followed by siliceous hydrogarnet, which is calculated to be present in the whole temperature range as a result of the hydration of ferrite and belite. Depending on the temperature, the hydration state of monosulfate can vary [68]. At lower temperature, monosulfate with 14 water ($C_4A\bar{S}H_{14}$) is predicted, while above 20 °C, rather monosulfate with 16 water ($C_4A\bar{S}H_{16}$) is calculated. Aluminium hydroxide is predicted to be absent at the high reaction degrees considered.

For BYF-Y (Fig. 21b), the calculated phases are siliceous hydrogarnet, C-S-H, strätlingite, ettringite, monosulfate and hydrotalcite. Note, as we have neglected the Al-uptake in C-S-H during the modelling due to lack of experimental data, we most probably over-predict the amount of strätlingite. The calculated amounts of phases do not change significantly with temperature. The amounts of strätlingite, C-S-H and siliceous hydrogarnet remain almost the same over the temperature range between 0 and 85 ºC, while the quantity of ettringite decreases and monosulfate increases with temperature. The amount of pore solution is lower in comparison to BYF-B due to the presence of more water-rich

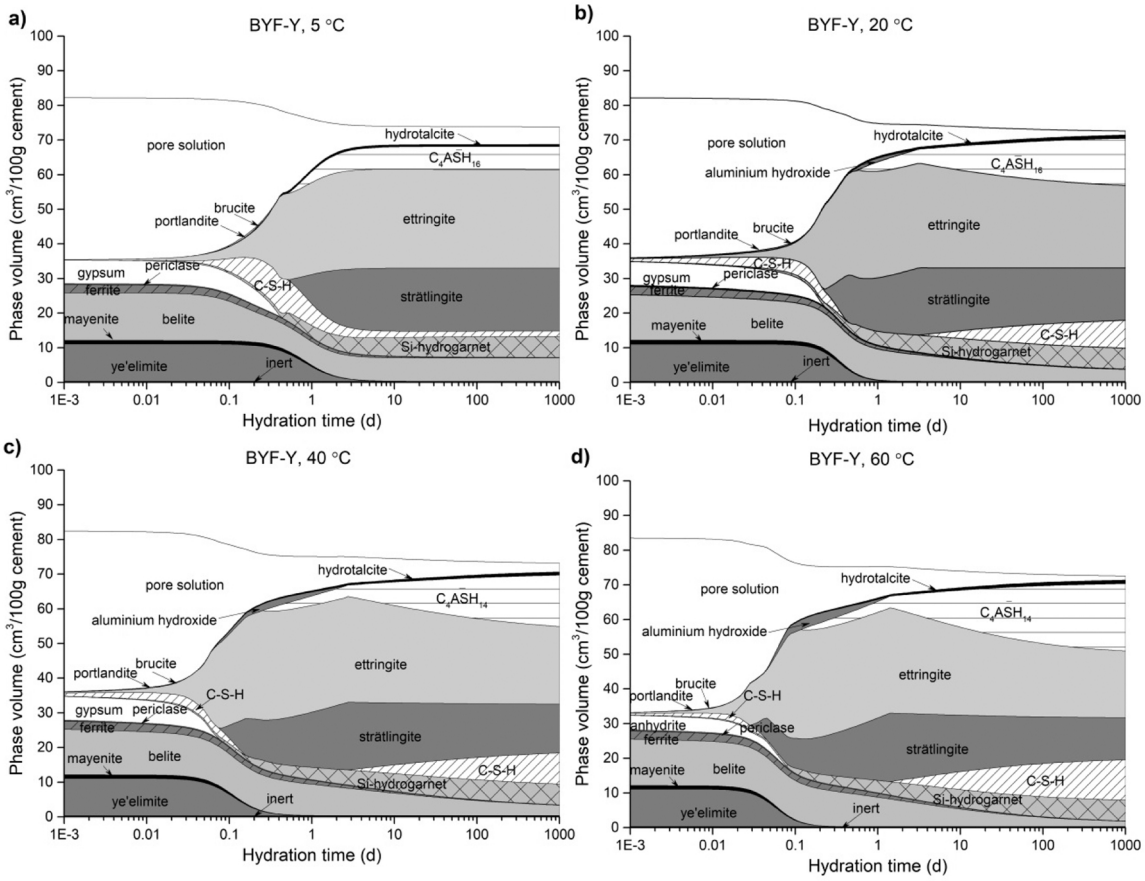

Fig. 18. Thermodynamic models of the phase assemblages as a function of hydration time at 5 °C (a), 20 °C (b), 40 °C (c) and 60 °C (d) for the BYF-Y cement.

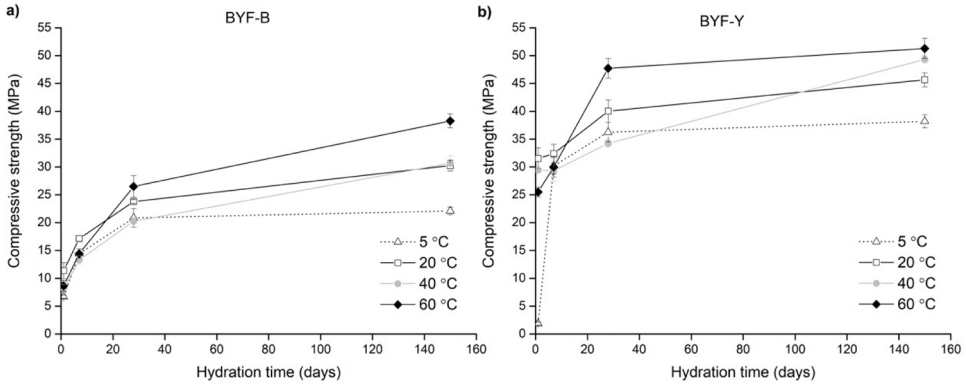

Fig. 19. Development of the compressive strength of BYF-B (a) and BYF-Y (b) cement at different curing temperatures. Data at 20 ºC were taken from [26].

ettringite and is slightly increasing with higher temperatures. The higher content of ye'elimite in cement BYF-Y results in more ettringite and strätlingite than for BYF-B, while the lower content of belite in BYF-Y leads to the prediction of less C-S-H.

These observations agree well with the long-term composition observed experimentally, with the exception of hydrogarnet, where we have observed experimentally more hydrogarnet at higher temperatures. This difference is related due to the slow formation kinetics of hydrogarnet at increased temperatures due to kinetic reasons [16,61], while during thermodynamic modelling immediate precipitation was assumed at all temperatures.

4. Conclusions

Different curing temperatures change the type of hydrates and their amounts. Higher temperatures expedite the dissolution of anhydrous phases, which is noticeable the most in ye'elimite hydration. At 5 °C, the hydration degrees of ye'elimite, gypsum and belite are lower in comparison to ambient and elevated temperatures. Belite reaction is promoted in the first 24 h, later it slows down, however it still reaches a degree of nearly 90% after 150 days at 60 °C. In contrast, the reaction degree of belite at 5 °C is only around 50% at 150 days.

At 20, 40 and 60 °C more monosulfate but less ettringite precipitates in BYF cements due to the increase of ettringite solubility with temperatures, while at 5 °C a high amount of ettringite is present.

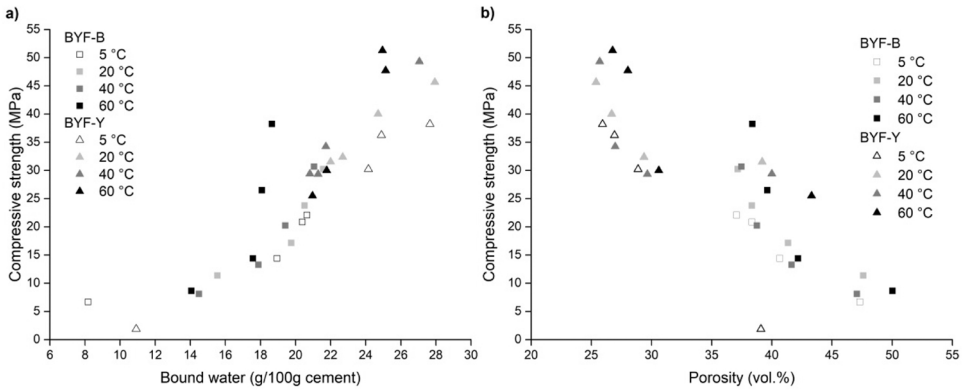

Fig. 20. (a) Bound water determined by TGA versus measured compressive strength for BYF-B and BYF-Y. (b) Calculated total porosity derived from thermodynamic modelling versus measured compressive strength for BYF-B and BYF-Y. Data at 20 ºC were taken from [26].

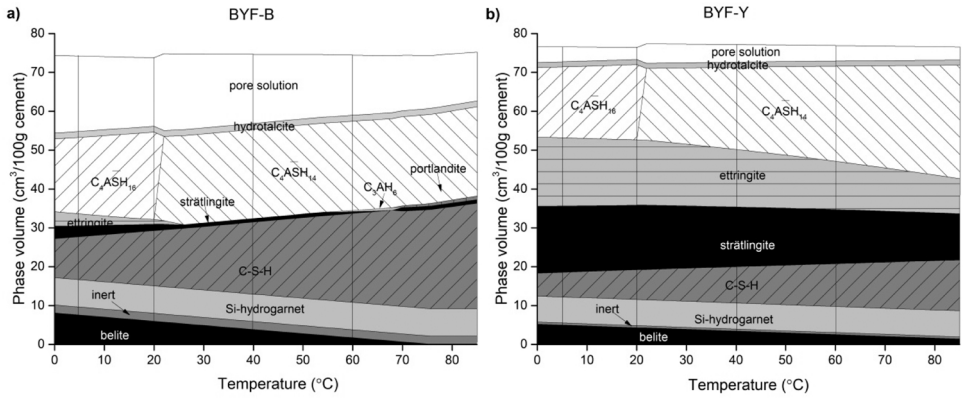

Fig. 21. Calculated phase assemblages in cm^3 per 100 g unhydrated cement for the belite-rich BYF-B (a) and the ye'elimite-rich BYF-Y (b) cements, as a function of temperature. The lines indicate the samples studied experimentally at 5, 20, 40 and 60 ºC. The ye'elimite, ferrite, periclase and mayenite reaction degrees of 100% correspond to the reaction degree observed at approximately 150 days as discussed in Section 3.3. The reaction degree of belite was assumed to increase linearly with temperature based on X-ray diffraction data.

Precipitation of aluminium hydroxide is associated to the hydration of ye'elimite and its formation is observed at early reaction times only, while aluminium is taken up in C−S−H, siliceous hydrogarnet and AFm-phases at later ages once belite and ferrite have reacted to some extent. Even though belite hydration is slower at low temperatures, the amount of strätlingite is decreasing at elevated temperatures, due to the formation of siliceous hydrogarnet, which takes up aluminium from strätlingite. Siliceous hydrogarnet formation is favoured by increased temperatures, and is not detected at 5 °C. More C−S−H precipitated according to EDS analysis at higher temperature as more belite reacted.

At low temperatures (5 °C) the microstructure is denser and the distribution of hydration products is more homogenous due to the slower hydration, while with increasing temperature from 20° to 60°C the microstructure becomes more and more heterogeneous and the hydration products can easily be differentiated. Less anhydrous grains are visible with increasing temperature, indicating a higher degree of hydration. C−S−H is found in the interstitial free space between grains of ettringite and monosulfate.

Early compressive strength is significantly lower at 5 ºC in comparison to 20, 40 and 60 ºC. At late ages, the compressive strength increases at higher curing temperatures due to the increased hydration of belite at elevated temperatures which forms strätlingite, C−S−H and siliceous hydrogarnet. Compressive strength shows a positive correlation with bound water and a negative correlation to the calculated total porosity determined from thermodynamic modelling.

Thermodynamic modelling confirmed that temperature mainly affects the reaction kinetics of belite-ye'elimite-ferrite cements and much less the kind of hydrates formed. Hydration kinetics is accelerated when the curing temperature is increased. At 5 °C the hydration is rather slow, while at elevated temperatures the clinker reactions occur significantly faster. The experimental results agree well with thermodynamic modelling, where in addition to ettringite aluminium hydroxide, monosulfate, strätlingite, C–S–H and siliceous hydrogarnet are calculated as stable main hydrate phases at all temperatures. As minor phases hydrotalcite, portlandite and brucite were calculated. With increasing temperature less ettringite and more monosulfate are predicted. Furthermore, higher amounts of C−S−H are calculated at elevated temperatures due to the higher reaction degree of belite.

Finally, the results also show that the composition of the cement clinker affects the kind and amount of hydrates formed. At early times, more heat is generated and more bound water is observed in the ye'elimite-rich BYF-Y in comparison to BYF-B, as more ettringite is formed in clinker BYF-Y. Also, compressive strength is higher in BYF-Y than in BYF-B, due to the presence of more ettringite both at early and late times. More strätlingite precipitates in cement BYF-Y with a higher amount of ye'elimite, while in the belite-rich BYF-B more siliceous hydrogarnet and C−S−H has formed due to the higher availability of calcium. This trend is more pronounced at elevated temperatures, where a higher amount of strätlingite is detected in BYF-Y than in BYF-B.

CRediT authorship contribution statement

Legat Andraž: Writing – review & editing. **Dolenec Sabina:** Writing – review & editing, Writing – original draft, Validation, Supervision,

Methodology, Conceptualization. **Mrak Maruša:** Writing – review & editing, Writing – original draft, Validation, Software, Methodology, Investigation, Formal analysis, Data curation, Conceptualization. **Winnefeld Frank:** Writing – review & editing, Writing – original draft, Validation, Supervision, Software, Methodology, Conceptualization. **Lothenbach Barbara:** Writing – review & editing, Writing – original draft, Validation, Supervision, Software, Methodology, Conceptualization.

Declaration of Competing Interest

The authors declare that they have no known competing financial interests or personal relationships that could have appeared to influence the work reported in this paper.

Data availability

No data was used for the research described in the article.

Acknowledgements

The research is performed within the Young Researcher Programme and is financially supported by the Slovenian Research Agency, contract number 1000-18-1502. The research is also a part of NanoCEM partner project: Influence of temperature on the hydration of belite-calcium sulfoaluminate cements (2018–2021).

Appendix A. Supporting information

Supplementary data associated with this article can be found in the online version at doi:10.1016/j.conbuildmat.2023.134260.

References

[1] B. Lothenbach, F. Winnefeld, C. Alder, E. Wieland, P. Lunk, Effect of temperature on the pore solution, microstructure and hydration products of Portland cement pastes, Cem. Conc. Res. 37 (2007) 483–491, https://doi.org/10.1016/j.cemconres.2006.11.016.
[2] B. Lothenbach, T. Matschei, G. Möschner, F.P. Glasser, Thermodynamic modelling of the effect of temperature on the hydration and porosity of Portland cement, Cem. Conc. Res. 38 (2008) 1–18, https://doi.org/10.1016/j.cemconres.2007.08.017.
[3] J.I. Escalante-García, J.H. Sharp, Effect of temperature on the hydration of the main clinker phases in portland cements: part i, neat cements, Cem. Conc. Res. 28 (1998) 1245–1257, https://doi.org/10.1016/S0008-8846(98)00115-X.
[4] E. Gallucci, X. Zhang, K.L. Scrivener, Effect of temperature on the microstructure of calcium silicate hydrate (C-S-H), Cem. Conc. Res. 53 (2013) 185–195, https://doi.org/10.1016/j.cemconres.2013.06.008.
[5] F. Deschner, B. Lothenbach, F. Winnefeld, J. Neubauer, Effect of temperature on the hydration of Portland cement blended with siliceous fly ash, Cem. Conc. Res. 52 (2013) 169–181, https://doi.org/10.1016/j.cemconres.2013.07.006.
[6] J.I. Escalante-García, J.H. Sharp, The microstructure and mechanical properties of blended cements hydrated at various temperatures, Cem. Conc. Res. 31 (2001) 695–702, https://doi.org/10.1016/S0008-8846(01)00471-9.
[7] I. Elkhadiri, F. Puertas, The effect of curing temperature on sulphate-resistant cement hydration and strength, Constr. Build. Mater. 22 (2008) 1331–1341, https://doi.org/10.1016/j.conbuildmat.2007.04.014.
[8] I. Elkhadiri, M. Palacios, F. Puertas, Effect of curing temperature on cement hydration, Ceram. Silik. 53 (2009) 65–75.
[9] W. Ma, D. Sample, I.R. Martin, P.W. Brown, Calorimetric study of cement blends containing fly ash, silica fume, and slag at elevated temperatures, Cem. Concr. Aggreg. 16 (1994) 7.
[10] J.I. Escalante-Garcia, J.H. Sharp, The effect of temperature on the early hydration of Portland cement and blended cements, Adv. Cem. Res. 12 (2000) 121–130, https://doi.org/10.1680/adcr.2000.12.3.121.
[11] K.O. Kjellsen, R.J. Detwiler, O.E. Gjørv, Development of microstructures in plain cement pastes hydrated at different temperatures, Cem. Conc. Res. 21 (1991) 179–189, https://doi.org/10.1016/0008-8846(91)90044-I.
[12] R.B. Perkins, C.D. Palmer, Solubility of ettringite (Ca6[Al(OH)6]2(SO4)3·26H2O) at 5–75°C, Geochim. Et. Cosmochim. Acta 63 (1999) 1969–1980, https://doi.org/10.1016/S0016-7037(99)00078-2.
[13] B. Lothenbach, D.A. Kulik, T. Matschei, M. Balonis, L. Baquerizo, B. Dilnesa, G. D. Miron, R.J. Myers, Cemdata18: a chemical thermodynamic database for hydrated Portland cements and alkali-activated materials, Cem. Conc. Res. 115 (2019) 472–506, https://doi.org/10.1016/j.cemconres.2018.04.018.
[14] F. Avet, K. Scrivener, Effect of temperature on the water content of C-A-S-H in plain Portland and blended cements, Cem. Conc. Res. 136 (2020), 106124, https://doi.org/10.1016/j.cemconres.2020.106124.
[15] A. Bentur, R.L. Berger, J.H. Kung, N.B. Milestone, J.F. Young, Structural properties of calcium silicate pastes: II, effect of curing temperature, J. Am. Ceram. Soc. 62 (1979) 362–366, https://doi.org/10.1111/j.1151-2916.1979.tb19079.x.
[16] P. Wang, N. Li, L. Xu, Hydration evolution and compressive strength of calcium sulphoaluminate cement constantly cured over the temperature range of 0 to 80°C, Cem. Conc. Res. 100 (2017) 203–213, https://doi.org/10.1016/j.cemconres.2017.05.025.
[17] L. Xu, S. Liu, N. Li, Y. Peng, K. Wu, P. Wang, Retardation effect of elevated temperature on the setting of calcium sulfoaluminate cement clinker, Constr. Build. Mater. 178 (2018) 112–119, https://doi.org/10.1016/j.conbuildmat.2018.05.061.
[18] L. Zhang, F.P. Glasser, Hydration of calcium sulfoaluminate cement at less than 24h, Adv. Cem. Res. 14 (2002) 15, https://doi.org/10.1680/adcr.2002.14.4.141.
[19] J. Kaufmann, F. Winnefeld, B. Lothenbach, Stability of ettringite in CSA cement at elevated temperatures, Adv. Cem. Res. 28 (2016) 251–261, https://doi.org/10.1680/jadcr.15.00029.
[20] Y. Jeong, C.W. Hargis, H. Kang, S.-C. Chun, J. Moon, The effect of elevated curing temperatures on high Ye'elimite calcium sulfoaluminate cement mortars, Mater 12 (2019) 1072, https://doi.org/10.3390/ma12071072.
[21] L. Li, R. Wang, S. Zhang, Effect of curing temperature and relative humidity on the hydrates and porosity of calcium sulfoaluminate cement, Constr. Build. Mater. 213 (2019) 627–636, https://doi.org/10.1016/j.conbuildmat.2019.04.044.
[22] N. Chitvoranund, Stability of hydrate assemblages and properties of cementitious systems with higher alumina content, EPFL, 2021.
[23] I.A. Chen, M.C.G. Juenger, Synthesis and hydration of calcium sulfoaluminate-belite cements with varied phase compositions, J. Mater. Sci. 46 (2011) 2568–2577, https://doi.org/10.1007/s10853-010-5109-9.
[24] M. Borštnar, N. Daneu, S. Dolenec, Phase development and hydration kinetics of belite-calcium sulfoaluminate cements at different curing temperatures, Ceram. Int. 46 (2020) 29421–29428, https://doi.org/10.1016/j.ceramint.2020.05.029.
[25] M. Borštnar, C.L. Lengauer, S. Dolenec, Quantitative in Situ X-ray diffraction analysis of early hydration of belite-calcium sulfoaluminate cement at various defined temperatures, Minerals 11 (2021) 297, https://doi.org/10.3390/min11030297.
[26] M. Mrak, F. Winnefeld, B. Lothenbach, S. Dolenec, The influence of calcium sulfate content on the hydration of belite-calcium sulfoaluminate cements with different clinker phase compositions, Mater. Struct. 54 (2021), 212, https://doi.org/10.1617/s11527-021-01811-w.
[27] R. Snellings, J. Chwast, Ö. Cizer, N. Belie, Y. Dhandapani, P. Durdziński, J. Elsen, J. Haufe, D. Hooton, C. Patapy, M. Santhanam, K. Scrivener, D. Snoeck, L. Steger, S. Tongbo, A. Vollpracht, F. Winnefeld, B. Lothenbach, RILEM TC-238 SCM recommendation on hydration stoppage by solvent exchange for the study of hydrate assemblages, Mater. Struct. 51 (2018), https://doi.org/10.1617/s11527-018-1298-5.
[28] R. Snellings, X-ray powder diffraction applied to cement. A Practical Guide to Microstructural Analysis of Cementitious Materials, first ed., CRCPress, 2016, pp. 126–195, https://doi.org/10.1201/b19074-4.
[29] A. Cuesta, Á.G. De la Torre, E.R. Losilla, I. Santacruz, M.A.G. Aranda, Pseudocubic crystal structure and phase transition in doped Ye'elimite, Cryst. Growth Des. 14 (2014) 5158–5163, https://doi.org/10.1021/cg501290q.
[30] A. Cuesta, A.G. De la Torre, E.R. Losilla, V.K. Peterson, P. Rejmak, A. Ayuela, C. Frontera, M.A.G. Aranda, Structure, atomistic simulations, and phase transition of stoichiometric Yeelimite, Chem. Mater. 25 (2013) 1680–1687, https://doi.org/10.1021/cm400129z.
[31] D. Jansen, F. Goetz-Neunhoeffer, C. Stabler, J. Neubauer, A remastered external standard method applied to the quantification of early OPC hydration, Cem. Conc. Res. 41 (2011) 602–608, https://doi.org/10.1016/j.cemconres.2011.03.004.
[32] D. Jansen, Ch Stabler, F. Goetz-Neunhoeffer, S. Dittrich, J. Neubauer, Does ordinary Portland cement contain amorphous phase? a quantitative study using an external standard method, Powder Diffr. 26 (2011) 31–38, https://doi.org/10.1154/1.3549186.
[33] B.H. O'Connor, M.D. Raven, Application of the Rietveld refinement procedure in assaying powdered mixtures, Powder Diffr. 3 (1988) 2–6, https://doi.org/10.1017/S0885715600013026.
[34] B. Lothenbach, P. Durdzinski, K. De Weerdt, Thermogravimetric analysis. A Practical Guide to Microstructural Analysis of Cementitious Materials, first ed., CRC Press, 2016.
[35] T. Wagner, D.A. Kulik, F.F. Hingerl, S.V. Dmytrieva, GEM-selektor geochemical modeling package: TSolMod library and data interface for multicomponent phase models, Contrib. Can. Mineral. 50 (2012) 1173–1195, https://doi.org/10.3749/canmin.50.5.1173.
[36] D.A. Kulik, T. Wagner, S.V. Dmytrieva, G. Kosakowski, F.F. Hingerl, K. V. Chudnenko, U. Berner, GEM-selektor geochemical modeling package: revised algorithm and GEMS3K numerical kernel for coupled simulation codes, Comput. Geosci. 17 (2013) 1–24, https://doi.org/10.1007/s10596-012-9310-6.
[37] D.A. Kulik, Improving the structural consistency of C-S-H solid solution thermodynamic models, Cem. Conc. Res. 41 (2011) 477–495, https://doi.org/10.1016/j.cemconres.2011.01.012.
[38] D.A. Kulik, F. Winnefeld, A. Kulik, G.D. Miron, B. Lothenbach, CemGEMS – an easy-to-use web application for thermodynamic modeling of cementitious materials, RILEM Tech. Lett. 6 (2021) 36–52, https://doi.org/10.21809/rilemtechlett.2021.140.

[39] N. Chitvoranund, F. Winnefeld, C.W. Hargis, S. Sinthupinyo, B. Lothenbach, Synthesis and hydration of alite-calcium sulfoaluminate cement, Adv. Cem. Res. 29 (2017) 101–111, https://doi.org/10.1680/jadcr.16.00071.
[40] F. Winnefeld, L.H.J. Martin, C.J. Müller, B. Lothenbach, Using gypsum to control hydration kinetics of CSA cements, Constr. Build. Mater. 155 (2017) 154–163, https://doi.org/10.1016/j.conbuildmat.2017.07.217.
[41] D. Jansen, A. Spies, J. Neubauer, D. Ectors, F. Goetz-Neunhoeffer, Studies on the early hydration of two modifications of ye'elimite with gypsum, Cem. Conc. Res. 91 (2017) 106–116, https://doi.org/10.1016/j.cemconres.2016.11.009.
[42] A. Rungchet, C.S. Poon, P. Chindaprasirt, K. Pimraksa, Synthesis of low-temperature calcium sulfoaluminate-belite cements from industrial wastes and their hydration: comparative studies between lignite fly ash and bottom ash, Cem. Concr. Compos. 83 (2017) 10–19, https://doi.org/10.1016/j.cemconcomp.2017.06.013.
[43] Y. Shen, X. Li, X. Chen, W. Zhang, D. Yang, Synthesis and calorimetric study of hydration behavior of sulfate-rich belite sulfoaluminate cements with different phase compositions, J. Therm. Anal. Calor. 133 (2018) 1281–1289, https://doi.org/10.1007/s10973-018-7251-6.
[44] F. Winnefeld, S. Barlag, Calorimetric and thermogravimetric study on the influence of calcium sulfate on the hydration of ye'elimite, J. Therm. Anal. Calor. 101 (2010) 949–957, https://doi.org/10.1007/s10973-009-0582-6.
[45] L. Pelletier-Chaignat, F. Winnefeld, B. Lothenbach, C.J. Müller, Beneficial use of limestone filler with calcium sulphoaluminate cement, Constr. Build. Mater. 26 (2012) 619–627, https://doi.org/10.1016/j.conbuildmat.2011.06.065.
[46] S. Shirani, A. Cuesta, A. Morales-Cantero, A.G. De la Torre, M.P. Olbinado, M.A. G. Aranda, Influence of curing temperature on belite cement hydration: a comparative study with Portland cement, Cem. Conc. Res. 147 (2021), 106499, https://doi.org/10.1016/j.cemconres.2021.106499.
[47] N. Li, L. Xu, R. Wang, L. Li, P. Wang, Experimental study of calcium sulfoaluminate cement-based self-leveling compound exposed to various temperatures and moisture conditions: hydration mechanism and mortar properties, Cem. Conc. Res. 108 (2018) 103–115, https://doi.org/10.1016/j.cemconres.2018.03.012.
[48] F. Winnefeld, B. Lothenbach, Hydration of calcium sulfoaluminate cements — experimental findings and thermodynamic modelling, Cem. Conc. Res. 40 (2010) 1239–1247, https://doi.org/10.1016/j.cemconres.2009.08.014.
[49] I.A. Chen, M.C.G. Juenger, Incorporation of coal combustion residuals into calcium sulfoaluminate-belite cement clinkers, Cem. Concr. Compos. 34 (2012) 893–902, https://doi.org/10.1016/j.cemconcomp.2012.04.006.
[50] S. Berger, C.C.D. Coumes, P. Le Bescop, D. Damidot, Influence of a thermal cycle at early age on the hydration of calcium sulphoaluminate cements with variable gypsum contents, Cem. Conc. Res. 41 (2011) 149–160, https://doi.org/10.1016/j.cemconres.2010.10.001.
[51] A.J.M. Cuberos, Á.G. De la Torre, G. Álvarez-Pinazo, M.C. Martín-Sedeño, K. Schollbach, H. Pöllmann, M.A.G. Aranda, Active iron-rich belite sulfoaluminate cements: clinkering and hydration, Environ. Sci. Technol. 44 (2010) 6855–6862, https://doi.org/10.1021/es101785n.
[52] G. Álvarez-Pinazo, I. Santacruz, M.A.G. Aranda, Á.G. De la Torre, Hydration of belite–ye'elimite–ferrite cements with different calcium sulfate sources, Adv. Cem. Res. 28 (2016) 529–543, https://doi.org/10.1680/jadcr.16.00030.
[53] M. García-Maté, A.G. De la Torre, L. León-Reina, E.R. Losilla, M.A.G. Aranda, I. Santacruz, Effect of calcium sulfate source on the hydration of calcium sulfoaluminate eco-cement, Cem. Concr. Compos. 55 (2015) 53–61, https://doi.org/10.1016/j.cemconcomp.2014.08.003.
[54] A. Telesca, M. Marroccoli, M.L. Pace, M. Tomasulo, G.L. Valenti, P.J.M. Monteiro, A hydration study of various calcium sulfoaluminate cements, Cem. Concr. Compos. 53 (2014) 224–232, https://doi.org/10.1016/j.cemconcomp.2014.07.002.
[55] G.S. Li G. Walenta E. Gartner Formation and hydration of low CO2 cements based on belite, calcium sulfoaluminate and calcium aluminoferrite, in: Proceedings of the 12th ICCC, Montreal, Canada 2007 9 12.(pp).
[56] M. Zajac, J. Skocek, C. Stabler, F. Bullerjahn, M. Ben Haha, Hydration and performance evolution of belite-ye'elimite-ferrite cement, Adv. Cem. Res. 31 (2019) 124–137, https://doi.org/10.1680/jadcr.18.00110.
[57] K. Scrivener, R. Snellings, B. Lothenbach. A Practical Guide to Microstructural Analysis of Cementitious Materials, first ed., CRC Press, Boca Raton, 2016.
[58] V. Morin, P. Termkhajornkit, B. Huet, G. Pham, Impact of quantity of anhydrite, water to binder ratio, fineness on kinetics and phase assemblage of belite-ye'elimite-ferrite cement, Cem. Concr. Res. 99 (2017) 8–17, https://doi.org/10.1016/j.cemconres.2017.04.014.
[59] D. Gastaldi, G. Paul, L. Marchese, S. Irico, E. Boccaleri, S. Mutke, L. Buzzi, F. Canonico, Hydration products in sulfoaluminate cements: evaluation of amorphous phases by XRD/solid-state NMR, Cem. Conc. Res. 90 (2016) 162–173, https://doi.org/10.1016/j.cemconres.2016.05.014.
[60] M. Ben Haha, F. Winnefeld, A. Pisch, Advances in understanding ye'elimite-rich cements, Cem. Conc. Res. 123 (2019), 105778, https://doi.org/10.1016/j.cemconres.2019.105778.
[61] B.Z. Dilnesa, B. Lothenbach, G. Renaudin, A. Wichser, D. Kulik, Synthesis and characterization of hydrogarnet Ca3(AlxFe1−x)2(SiO4)y(OH)4(3−y), Cem. Conc. Res. 59 (2014) 96–111, https://doi.org/10.1016/j.cemconres.2014.02.001.
[62] K. De Weerdt, M. Ben Haha, G. Le Saout, K.O. Kjellsen, H. Justnes, B. Lothenbach, The effect of temperature on the hydration of composite cements containing limestone powder and fly ash, Mater. Struct. 45 (2012) 1101–1114, https://doi.org/10.1617/s11527-011-9819-5.
[63] K.L. Scrivener, Backscattered electron imaging of cementitious microstructures: understanding and quantification, Cem. Concr. Compos. 26 (2004) 935–945, https://doi.org/10.1016/j.cemconcomp.2004.02.029.
[64] Y. Jeong, C.W. Hargis, S.-C. Chun, J. Moon, The effect of water and gypsum content on strätlingite formation in calcium sulfoaluminate-belite cement pastes, Constr. Build. Mater. 166 (2018) 712–722, https://doi.org/10.1016/j.conbuildmat.2018.01.153.
[65] B. Lothenbach, B. Albert, M. Vincent, G. Ellis, Hydration of Belite-Ye'elimite-Ferrite cements: thermodynamic modeling, in: 14th International Conference on the Chemistry of Cement, Beijing, China, 2015: p. 12.
[66] T. Sui, L. Fan, Z. Wen, J. Wang, Properties of belite-rich Portland cement and concrete in China, J. Civ. Eng. Archit. 9 (2015), https://doi.org/10.17265/1934-7359/2015.04.002.
[67] T. Sui, L. Fan, Z. Wen, J. Wang, Z. Zhang, Study on the properties of high strength concrete using high belite cement, ACT 2 (2004) 201–206, https://doi.org/10.3151/jact.2.201.
[68] L.G. Baquerizo, T. Matschei, K.L. Scrivener, M. Saeidpour, L. Wadsö, Hydration states of AFm cement phases, Cem. Conc. Res. 73 (2015) 143–157, https://doi.org/10.1016/j.cemconres.2015.02.011.